SCIENCE CHINA
Information Sciences

• RESEARCH PAPER •

May 2022, Vol. 65 152305:1–152305:19
https://doi.org/10.1007/s11432-020-3250-7

Range-angle-dependent beamforming for FDA-MIMO radar using oblique projection

Lan LAN[1*], Guisheng LIAO[1], Jingwei XU[1*], Shengqi ZHU[1] & Yuhong ZHANG[2]

[1]*National Key Laboratory of Radar Signal Processing, Xidian University, Xi'an* 710071*, China;*
[2]*School of Electronic Engineering, Xidian University, Xi'an* 710071*, China*

Received 25 November 2020/Revised 23 February 2021/Accepted 21 April 2021/Published online 18 April 2022

Abstract Frequency diverse array (FDA)-multiple-input and multiple-output (MIMO) radar is characterized with a range-angle-dependent transceive beampattern by introducing incremental frequencies among the transmit array elements and separating the transmitted waveforms with matched filtering in the receiver. In this respect, the paper aims to control the range-angle-dependent transceive beampattern for FDA-MIMO radar by designing the weight vector according to the desired response. At the design stage, the weight vectors to control the beampattern responses of different regions are devised by performing the orthogonal decomposition technique. Then, a filtering matrix using the oblique projection operator is constructed to filter the weight vectors for different regions, where two iterative algorithms are developed either considering concurrent or successive control of multiple regions. In such a way, a desired range-angle-dependent transceive beampattern is formed with simultaneously broadened nulls and a flat-top mainlobe. At the analysis stage, the method has been applied to interference mitigation in FDA-MIMO radar, where the mismatch exists both in the sidelobes and mainlobe. Simulated and measured results are provided to corroborate the effectiveness of the proposed methods.

Keywords FDA-MIMO radar, range-angle-dependent beamforming, weight vector orthogonal decomposition, oblique projection, interference mitigation

Citation Lan L, Liao G S, Xu J W, et al. Range-angle-dependent beamforming for FDA-MIMO radar using oblique projection. Sci China Inf Sci, 2022, 65(5): 152305, https://doi.org/10.1007/s11432-020-3250-7

1 Introduction

The frequency diverse array (FDA) radar has been widely studied and applied in many applications owing to the increased degrees-of-freedom (DOFs) in the range domain, providing more flexibility in system design and signal processing [1–6]. Different from the phased array radar, where the transmit beampattern is only angle-dependent, the transmit beampattern of FDA is range-angle-time-dependent, which has been widely studied during the past few years [7, 8]. However, in standard FDA, frequencies of elements are increased linearly, which yields a coupled 'S'-shape beampattern in the joint angle-range domain, leading to possible ambiguities in the range-angle dimension during the target localization process [9]. Besides, the time-variant beampattern is not desired for target localization in practice, which means that any radiation/waveform/peak/null experienced at a certain point of range will travel to any points along the same direction [10–12]. To overcome these drawbacks, the multiple-input multiple-output (MIMO) technique is combined with the FDA. In FDA-MIMO radar, the orthogonal waveforms are transmitted, then, after matched filtering in the receiver, the transmitted waveforms are separated. Hence, the time-independent beampattern can be obtained, which is different from the coherent FDA. Hence, the range-angle-dependent transceive beampattern of FDA-MIMO radar is achieved, which can be used to solve problems that the conventional MIMO radar cannot handle [13–16]. Although many efforts have been devoted to FDA-MIMO radar by utilizing extra DOFs in various applications, it still calls for sophisticated transceive beamforming to maintain low sidelobes for interference suppression in dynamic environments, where the time-varying interferences lead to a mismatch in nulling angles.

* Corresponding author (email: lanlan@xidian.edu.cn, xujingwei1987@163.com)

To the best of the authors' knowledge, the design of the transceive beampattern has only received a limited attention in the FDA-MIMO context. Specifically, a multisub-FDA scheme was proposed in [17] to generate range-angle-decoupled equivalent transmit beampattern with low sidelobes. However, it fails to control the null regions of the beampattern accurately. Artificial interferences with prescribed powers were added to form a trough-like transceive beampattern in [18], however, the proposed method filed to control the mainlobe of the beampattern. Hence, it is worth investigating the beampattern synthesis for exploiting specific peculiarities of the FDA-MIMO radar. The starting point is the inspiration offered by the plethora of beamforming methods that have been proposed in the open literature, where the weight vectors are adjusted according to the environment to extract the signal of interest (SOI) while handling the interferences from surroundings [19–22]. Generally, beamformers can be classified into the data-dependent beamformers (also known as the adaptive beamformers) and the data-independent beamformers. The adaptive beamformers using linearly constrained minimum variance (LCMV) [23], second-order cone programming (SOCP) [24], semidefinite relaxation (SDR) [25], projection beamforming [26], and the uncertainty set-based techniques [27], were developed to control the array response. Although good performance has been achieved in stationary state, they have to deal with difficulties such as uncertainties of directions-of-arrival (DOAs) and covariance matrix estimation.

To overcome the limitations of data-dependent beamforming and fulfill different application requirements,the data-independent beamforming techniques are becoming more and more important, especially in generating a particular beampattern shape without array training data. The adaptive array theory was applied to control sidelobes in [28–31]. Besides, to control the response of arbitrary arrays accurately, the accurate array response control (A^{2}RC) [32] and the weight vector orthogonal decomposition (WORD) [33] methods were proposed. However, they cannot always guarantee a satisfactory performance for a multi-dimensional beampattern. In addition, optimization algorithms, such as genetic algorithm [34], particle swarm optimization [35], and simulated annealing [36] were proposed to optimize the weight vectors directly. Nevertheless, they suffer from high computational complexity. Moreover, most of the beampattern synthesis methods deal with only the array factors without considering practical factors, which is not realistic in practice. Hence, sophisticated beampattern synthesis methods, with the FDA-MIMO framework combined, are supposed to be designed.

Aimed at forming a range-angle-dependent transceive beampattern for FDA-MIMO radar with desired response, methods based on beampattern synthesis are developed to control the response of the beampattern based on the adaptive beamforming theory in this paper. Firstly, the response of each region is adjusted based on weight vector orthogonal decomposition according to a predefined response. Then, a filtering matrix is constructed by virtue of an oblique projection operator to control multiple regions simultaneously. On this basis, two types of iterative algorithms with multiple-response control based on oblique projection (MRCOP) are developed, including the concurrent MRCOP (C-MRCOP) and the successive MRCOP (S-MRCOP). At the analysis stage, both simulated and measured data of the antenna beampattern are used to verify the performance of the designed transceive beampattern and interference suppression, where the broadened nulls are designed to suppress the interferences adequately and a flat-top mainlobe to extend receiving areas for the target.

The remainder of this paper is organized as follows. Section 2 presents the signal model of FDA-MIMO radar. The method to achieve single response control of the transceive beampattern using weight vector orthogonal decomposition is explored in Section 3. Methods to control multiple regions of the beampattern based on oblique projection are developed in Section 4. Numerical and measured results in Section 5 are provided to verify the performance of the proposed methods.

Notations. Boldfaced lowercase letters, such as $\boldsymbol{x}$, represent vectors, and boldfaced uppercase letters, such as $\boldsymbol{A}$, denote matrixes. For vector $\boldsymbol{x}$, we use $[\boldsymbol{x}]_n$ to denote the n-th element of vector $\boldsymbol{x}$. For matrix $\boldsymbol{A}$, we use $[\boldsymbol{A}]_{m,n}$ to denote the element of $\boldsymbol{A}$ in the m-th row and the n-th column, $[\boldsymbol{A}]_{m,:}$ to denote the m-th row vector of $\boldsymbol{A}$, and $[\boldsymbol{A}]_{:,n}$ to denote the n-th column vector of $\boldsymbol{A}$. $\boldsymbol{I}_N$, $\mathbf{1}_N$, and $\mathbf{0}_{M\times M}$ denote respectively the $N \times N$ identity matrix, $N \times 1$ vector with all elements being one, and $M \times M$ matrix with zero entries. $\mathbb{C}^N$, $\mathbb{R}^N$, $\mathbb{C}^{N\times M}$, and $\mathbb{H}^N$ are respectively the sets of N-dimensional vectors of complex numbers, N-dimensional vectors real numbers, $N \times M$ complex matrices, and $N \times N$ Hermitian matrices. For any $\boldsymbol{x} \in \mathbb{C}^N$, $\|\boldsymbol{x}\|$ indicates its Euclidian norm. $\mathrm{diag}(\boldsymbol{x})$ indicates the diagonal matrix whose i-th diagonal element is the i-th entry of $\boldsymbol{x}$. For any complex number z, $|z|$ indicates the modulus of z. The transpose, the conjugate, and the conjugate transpose operators are denoted by the symbols $(\cdot)^{\mathrm{T}}$, $(\cdot)^*$, and $(\cdot)^\dagger$, respectively. $\otimes$, $\odot$, and $\oslash$ represent the Kronecker product, the Hadamard product, and the division operator for elements from two matrixes. The letter j represents the imaginary unit

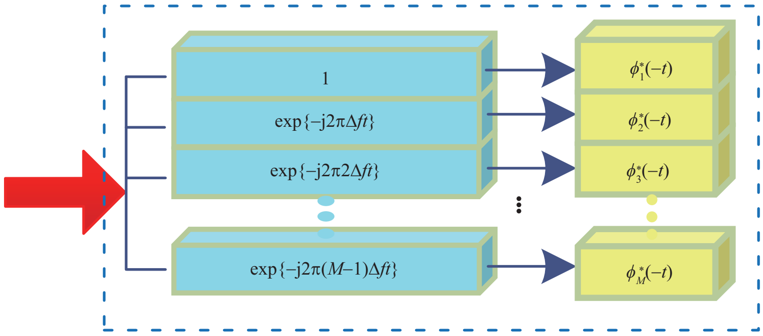

Figure 1 (Color online) Signal processing at the receiver in FDA-MIMO radar.

(i.e., $j=\sqrt{-1}$). Finally, $[a,b]$ indicates a region of the variable with a being the beginning and b being the end of the set.

2 Signal model of FDA-MIMO radar

Consider a uniform linear antenna array with M elements spaced by d. The same array is used for both transmission and reception, where the carrier frequency increases progressively across the transmit antenna elements with a small frequency increment Δf, and the frequency of the m-th element is expressed as follows:

$$f_m = f_0 + (m-1)\Delta f, \quad m = 1,2,\ldots,M, \tag{1}$$

where f_0 refers to the reference carrier frequency.

For a target located in the far-field at the angle θ_0 and range R_0, under the narrowband assumption, the reflected signal received by the n-th ($n=1,2,\ldots,M$) element is expressed as

$$\begin{aligned} y_n(t,\theta_0) &= \zeta \sum_{m=1}^{M} \phi_m(t-\tau_0)\mathrm{e}^{\mathrm{j}2\pi f_m (t-\tau_{m,n})} \\ &= \zeta \mathrm{e}^{\mathrm{j}2\pi f_0 (t-\tau_0)} \mathrm{e}^{\mathrm{j}2\pi \frac{d}{\lambda_0}(n-1)\sin(\theta_0)} \\ &\quad \sum_{m=1}^{M} \phi_m(t-\tau_0)\mathrm{e}^{\mathrm{j}2\pi\Delta f(m-1)(t-\tau_0)}\mathrm{e}^{\mathrm{j}2\pi(m-1)(n-1)\Delta f\frac{d}{c}\sin(\theta_0)}\mathrm{e}^{\mathrm{j}2\pi(m-1)^2\Delta f\frac{d}{c}\sin(\theta_0)}\mathrm{e}^{\mathrm{j}2\pi\frac{d}{\lambda_0}(m-1)\sin(\theta_0)} \\ &\approx \zeta \mathrm{e}^{\mathrm{j}2\pi f_0 (t-\tau_0)} \mathrm{e}^{\mathrm{j}2\pi \frac{d}{\lambda_0}(n-1)\sin(\theta_0)} \sum_{m=1}^{M} \phi_m(t-\tau_0)\mathrm{e}^{\mathrm{j}2\pi\Delta f(m-1)(t-\tau_0)}\mathrm{e}^{\mathrm{j}2\pi\frac{d}{\lambda_0}(m-1)\sin(\theta_0)}, \end{aligned} \tag{2}$$

where $\phi_m(t)$ is the m-th transmitted waveform, $\tau_{m,n} = \tau_0 - \frac{(m-1)d\sin\theta_0-(n-1)d\sin\theta_0}{c}$ is the round-trip propagation time delay, $\tau_0 = \frac{2R_0}{c}$ indicates the common time delay, ζ is the complex echo amplitude (accounting for the transmit amplitude, phase, target reflectivity, and channels propagation effects), $\lambda = \frac{c}{f_0}$ is the reference carrier wavelength, and the approximation holds when $(M-1)^2\Delta f\frac{d}{c} \ll 1$.

As shown in Figure 1, the received signals are first of all multiplied by $\mathrm{e}^{-\mathrm{j}2\pi f_0 t}$. Subsequently, on each receive channel, the echo is digitally mixed with $\mathrm{e}^{-\mathrm{j}2\pi(l-1)\Delta f t}$. Hence, the time-dependency is eliminated. Then, the signal on each receive channel is processed through a bank of M matched filters $h_l(t) = \phi_l^*(-t)$ ($l=1,\ldots,M$). Assume that the transmitted waveforms are orthogonal, after matched filtering with M waveforms, by stacking the received signals into an $M^2\times 1$ space-time snapshot, the received signal of the target can be expressed in a simple form as [14]

$$\boldsymbol{y}_{\mathrm{S}} = \alpha_0 \boldsymbol{a}_{\mathrm{T}}(\theta_0,R_0)\otimes \boldsymbol{b}_{\mathrm{R}}(\theta_0), \tag{3}$$

where $\alpha_0 = \zeta\mathrm{e}^{-\mathrm{j}2\pi\Delta f(m-1)\tau_0}$, $\boldsymbol{a}_{\mathrm{T}}(\theta_0,R_0)\in\mathbb{C}^M$, and $\boldsymbol{b}_{\mathrm{R}}(\theta_0)\in\mathbb{C}^M$ denote the transmit and receive steering vectors, respectively. Note that the owing to the procedure of digitally mixing with $\mathrm{e}^{-\mathrm{j}2\pi(l-1)\Delta f t}$ in the FDA-MIMO radar, the equivalent transmit steering vector $\boldsymbol{a}_{\mathrm{T}}(\theta_0,R_0)$ is time-independent. Please refer to Appendix A for detailed derivations.

Consider the pattern vector for each antenna element, the transmit and receive steering vectors can be written as

$$\boldsymbol{a}_{\mathrm{T}}(\theta_0,R_0)=\boldsymbol{g}(\theta_0)\odot(\mathrm{e}^{\mathrm{j}2\pi\boldsymbol{f}(R_0)}\cdot\mathrm{e}^{\mathrm{j}k(\theta_0)\boldsymbol{d}})=\begin{bmatrix} g_1(\theta_0)\mathrm{e}^{-\mathrm{j}\frac{2\pi}{\lambda}\cdot\frac{1}{2}(M-1)d\sin(\theta_0)} \\ \vdots \\ g_m(\theta_0)\mathrm{e}^{-\mathrm{j}2\pi\Delta f(m-1)\frac{2R_0}{c}}\mathrm{e}^{\mathrm{j}\frac{2\pi}{\lambda}(-\frac{1}{2}(M-1)+(m-1))d\sin(\theta_0)} \\ \vdots \\ g_M(\theta_0)\mathrm{e}^{-\mathrm{j}2\pi\Delta f(M-1)\frac{2R_0}{c}}\mathrm{e}^{\mathrm{j}\frac{2\pi}{\lambda}\cdot\frac{1}{2}(M-1)d\sin(\theta_0)} \end{bmatrix}, \tag{4a}$$

$$\boldsymbol{b}_{\mathrm{R}}(\theta_0)=\boldsymbol{g}(\theta_0)\odot\mathrm{e}^{\mathrm{j}k(\theta_0)\boldsymbol{d}}=\begin{bmatrix} g_1(\theta_0)\mathrm{e}^{-\mathrm{j}\frac{2\pi}{\lambda}\cdot\frac{1}{2}(M-1)d\sin(\theta_0)} \\ \vdots \\ g_n(\theta_0)\mathrm{e}^{\mathrm{j}\frac{2\pi}{\lambda}(-\frac{1}{2}(M-1)+(n-1))d\sin(\theta_0)} \\ \vdots \\ g_M(\theta_0)\mathrm{e}^{\mathrm{j}\frac{2\pi}{\lambda}\cdot\frac{1}{2}(M-1)d\sin(\theta_0)} \end{bmatrix}, \tag{4b}$$

where $\boldsymbol{f}(R_0)=[1,-\Delta f\frac{2R_0}{c},\ldots,-\Delta f(M-1)\frac{2R_0}{c}]^{\mathrm{T}}\in\mathbb{C}^M$ refers to the frequency increment vector of the target, $\boldsymbol{g}(\theta_0)=[g_1(\theta_0),g_2(\theta_0),\ldots,g_M(\theta_0)]^{\mathrm{T}}\in\mathbb{C}^M$ denotes the antenna element pattern vector, $k(\theta_0)=\frac{2\pi}{\lambda}\sin(\theta_0)$ is the wave number of the target, and $\boldsymbol{d}\in\mathbb{R}^M$ is the position vector of elements in the x-axis with the m-th position being $d_m=d(-\frac{1}{2}(M-1)+(m-1))$. It can be seen from (4a) that the transmit steering vector of FDA-MIMO is range-angle-dependent, while the receive steering vector is angle-dependent. Notice that when $\Delta f=0$ is considered, the equivalent beampattern degenerates into that of the conventional MIMO radar. For simplicity, consider an isotropic antenna array, i.e., $g_m(\theta_0)=1$, the transmit and receive steering vectors are respectively expressed as

$$\tilde{\boldsymbol{a}}_{\mathrm{T}}(\theta,R)=\boldsymbol{a}_{\mathrm{T}}(\theta,R)\oslash\boldsymbol{g}(\theta), \tag{5a}$$

$$\tilde{\boldsymbol{b}}_{\mathrm{R}}(\theta)=\boldsymbol{b}_{\mathrm{R}}(\theta)\oslash\boldsymbol{g}(\theta). \tag{5b}$$

3 Single response control of transceive beampattern

3.1 Motivations

Different from the angle-dependent transceive beampattern in the traditional MIMO radar, the range-angle-dependent transceive beampattern in FDA-MIMO radar can be utilized in mainlobe interference suppression, where the interference and the target are located at the same angle but different range. In this respect, the beampattern distortion occurs because the target is also suppressed when suppressing the interference with beamforming. However, owing to extra DOFs in the range domain in FDA-MIMO, the target and interferences can be distinguished in the joint range-angle-dependent transceive beampattern, and the interferences can be suppressed by nulling at the beampattern of the target [37]. However, under some mismatch circumstances, the interferences will not be exactly located at the nulls, especially in dynamic environments, the time-varying interferences lead to mismatches in nulling angles. Moreover, there will be a deviation from the mainlobe of the target. One feasible way to solve this problem is to design an appropriate range-angle-dependent transceive beampattern, where the broadened nulls is desired to suppress the interferences adequately, and a mainlobe with a flat top is required to extend receiving areas for the target.

Because the beampattern is formed according to the weight vector, the control of the beampattern can be accomplished by designing an appropriate weight vector to satisfy practical requirements. For a two-dimensional (2-D) range-angle-dependent transceive beampattern in FDA-MIMO radar, the optimal weight vector using the minimum variance distortionless response (MVDR) beamformer is constructed as follows:

$$\boldsymbol{w}_{\mathrm{opt}}=\Lambda\boldsymbol{R}_{j+n}^{-1}\boldsymbol{u}_0, \tag{6}$$

where $\boldsymbol{u}_0=\tilde{\boldsymbol{a}}_{\mathrm{T}}(\theta_0,R_0)\otimes\tilde{\boldsymbol{b}}_{\mathrm{R}}(\theta_0)\in\mathbb{C}^{M^2}$ denotes the transceive steering vector of the FDA-MIMO radar, $\boldsymbol{R}_{j+n}\in\mathbb{C}^{M^2\times M^2}$ refers to the interference-plus-noise matrix collected with several training samples, and

$\Lambda = (\boldsymbol{u}_0^\dagger \boldsymbol{R}_{j+n}^{-1} \boldsymbol{u}_0)^{-1}$ denotes a normalization factor. Although the requirements of the responses can be achieved using the convex optimization with multiple constraints, we focus on the data-independent beamformers to control the responses in this paper, where the adaptive array theory can be applied into data-independent beamformers.

3.2 Single response control using weight vector orthogonal decomposition

In this subsection, the control of a single response is considered. Assume that in a scenario with Gaussian white noise, there is a single interference. Hence, the jammer-plus-noise covariance matrix is described by

$$\boldsymbol{R}_{j+n} = \sigma_w^2 \boldsymbol{I}_{M^2} + \sigma_i^2 \boldsymbol{u}_i \boldsymbol{u}_i^\dagger, \tag{7}$$

where σ_w^2 and σ_i^2 refer to the power of noise and interference, respectively. The white Gaussian distributed noise is assumed with zero mean and variance σ_w^2. $\boldsymbol{u}_i = \tilde{\boldsymbol{a}}_{\mathrm{T}}(\theta_i, R_i) \otimes \tilde{\boldsymbol{b}}_{\mathrm{R}}(\theta_i) \in \mathbb{C}^{M^2}$ denotes the steering vector of the interference with θ_i and R_i being the angle and range of the interference, respectively. Using the matrix inversion lemma, the inverse of $\boldsymbol{R}_{j+n}$ is expressed as

$$\begin{aligned}
\boldsymbol{R}_{j+n}^{-1} &= \frac{1}{\sigma_w^2}\left[\boldsymbol{I}_{M^2} - \frac{\sigma_i^2}{\sigma_w^2 + \|\boldsymbol{u}_i\|_2^2 \sigma_i^2} \boldsymbol{u}_i \boldsymbol{u}_i^\dagger\right] \\
&= \frac{1}{\sigma_w^2}\left[\boldsymbol{I}_{M^2} - \boldsymbol{P}(\boldsymbol{u}_i) + \frac{\sigma_w^2}{\sigma_w^2 + \|\boldsymbol{u}_i\|_2^2 \sigma_i^2} \boldsymbol{P}(\boldsymbol{u}_i)\right] \\
&= \frac{1}{\sigma_w^2}[\boldsymbol{P}^\perp(\boldsymbol{u}_i) + \beta \boldsymbol{P}(\boldsymbol{u}_i)],
\end{aligned} \tag{8}$$

where $\beta = \frac{\sigma_w^2}{\sigma_w^2 + \|\boldsymbol{u}_i\|_2^2 \sigma_i^2}$, $\boldsymbol{P}(\boldsymbol{u}_i) = \frac{\boldsymbol{u}_i \boldsymbol{u}_i^\dagger}{\|\boldsymbol{u}_i\|_2^2} \in \mathbb{C}^{M^2 \times M^2}$ denotes the projection matrix which is projected onto the column space of $\boldsymbol{u}_i$, and $\boldsymbol{P}^\perp(\boldsymbol{u}_i) = \boldsymbol{I}_{M^2} - \boldsymbol{P}(\boldsymbol{u}_i) \in \mathbb{C}^{M^2 \times M^2}$. Thus, the normalized optimal weight vector is decomposed as

$$\begin{aligned}
\boldsymbol{w}_{\mathrm{opt}} &= \Lambda_0 \boldsymbol{R}_{j+n}^{-1} \boldsymbol{u}_0 \\
&= \frac{\Lambda_0}{\sigma_w^2}[\boldsymbol{P}^\perp(\boldsymbol{u}_i) + \beta \boldsymbol{P}(\boldsymbol{u}_i)]\boldsymbol{u}_0 \\
&= \alpha_0 \left[\boldsymbol{w}_0^\perp + \beta \boldsymbol{w}_0^\parallel\right],
\end{aligned} \tag{9}$$

where $\boldsymbol{w}_0^\parallel = \boldsymbol{P}(\boldsymbol{u}_i)\boldsymbol{u}_0 \in \mathbb{C}^{M^2}$, $\boldsymbol{w}_0^\perp = \boldsymbol{P}^\perp(\boldsymbol{u}_i)\boldsymbol{u}_0 \in \mathbb{C}^{M^2}$, $\alpha_0 = \frac{\Lambda_0}{\sigma_w^2}$, and $\Lambda_0 = \frac{\sigma_w^2}{\boldsymbol{u}_0^\dagger \boldsymbol{w}_0^\perp + \beta \boldsymbol{a}_0^\dagger \boldsymbol{w}_0^\parallel}$.

The response of the transceive beampattern at $\boldsymbol{u}_i$ is obtained as $B(\boldsymbol{u}_i|\boldsymbol{u}_0) = |\boldsymbol{w}_{\mathrm{opt}}^\dagger \boldsymbol{u}_i|^2$. Hence, for a fixed response ξ, by substituting the expression of $\boldsymbol{w}_{\mathrm{opt}}$ into $B(\boldsymbol{u}_i|\boldsymbol{u}_0)$, i.e., $|\boldsymbol{w}_{\mathrm{opt}}^\dagger \boldsymbol{u}_i|^2 = \xi$, it is obvious that $B(\boldsymbol{u}_i|\boldsymbol{u}_0)$ is a function of β. Note that according to the expression of β, it is related to the variances of the the noise and the interference, which cannot be directively estimated. In contrast, a closed-form of the solution to β can be obtained according to the prescribed response of the beampattern ξ. Consequently, the response control of the beampattern can be achieved by adjusting β.

Based on the previous discussions, for a specific single response, it can be accurately controlled by designing the weight vector which is decomposed as a linear combination of $\boldsymbol{w}_0^\perp$ and $\boldsymbol{w}_0^\parallel$ with a key coefficient β. However, for a given region Θ in the beampattern, multiple responses are supposed to be controlled together. In this regard, iterative algorithm can be performed to update the weight vector. Based on [33], it follows (9) that the weight vector in the l-th iteration is formulated as

$$\boldsymbol{w}_l = \alpha_l(\boldsymbol{w}_\perp + \beta_l \boldsymbol{w}_\parallel), \tag{10}$$

where $\boldsymbol{w}_\parallel \triangleq \boldsymbol{P}(\boldsymbol{u}_l)\boldsymbol{w}_{l-1} \in \mathbb{C}^{M^2}$, $\boldsymbol{w}_\perp \triangleq \boldsymbol{P}^\perp(\boldsymbol{u}_l)\boldsymbol{w}_{l-1} \in \mathbb{C}^{M^2}$, $\boldsymbol{u}_l \in \mathbb{C}^{M^2}$ denotes the steering vector of the point which is controlled in the l-th iteration, and $\alpha_l = \frac{1}{\boldsymbol{u}_0^\dagger \boldsymbol{w}_\perp + \beta_l \boldsymbol{u}_0^\dagger \boldsymbol{w}_\parallel}$. Notice that $\boldsymbol{w}_l$ is calculated to adjust the current response at $\boldsymbol{u}_l$. Different from [33] with angle-dependent steering vector, $\boldsymbol{u}_l$ indicates the range-angle-dependent transceive steering vector of the FDA-MIMO radar, where the range information is included. Besides, the weight vector in (10) is normalized.

With the expression of the weight vector, the response of the beampattern can be obtained, where $B(\boldsymbol{u}_l|\boldsymbol{u}_0)$ is used to denote a specific response of the beampattern evaluated at $\boldsymbol{u}_l$ and pointed towards

$\boldsymbol{u}_0$. In particular, the former within the bracket, i.e., $\boldsymbol{u}_l$, denotes the steering vector corresponding to the current response, while the latter, i.e., $\boldsymbol{u}_0$, represents the steering vector corresponding to the mainlobe. Given a desired beampattern response ξ, then, $B(\boldsymbol{u}_l|\boldsymbol{u}_0)$ is calculated as

$$B(\boldsymbol{u}_l|\boldsymbol{u}_0) = |\boldsymbol{w}_l^\dagger \boldsymbol{u}_l|^2 = \xi. \tag{11}$$

Particularly, in order to control the region Θ in the l-th iteration, the $\boldsymbol{u}_l$, where the response needs adjustment, should be chosen appropriately. One feasible way is to determine $\boldsymbol{u}_l$ according to the maximum difference between the current response of the beampattern and ξ within Θ, which can be categorized into two cases, i.e.,

$$\boldsymbol{u}_l = \mathop{\arg}_{\boldsymbol{u}_l \in \boldsymbol{u}_\Theta} \max \left| B\left(\boldsymbol{u}_l \left| \boldsymbol{u}_0 \right.\right) - \xi \right|, \quad \Theta = \Theta_{\mathrm{m}}, \tag{12a}$$

$$\boldsymbol{u}_l = \mathop{\arg}_{\boldsymbol{u}_l \in \boldsymbol{u}_\Theta} \max \left(B\left(\boldsymbol{u}_l \left| \boldsymbol{u}_0 \right.\right) - \xi, 0 \right), \quad \Theta \neq \Theta_{\mathrm{m}}, \tag{12b}$$

where $\boldsymbol{u}_\Theta \in \mathbb{C}^{M^2}$ denotes an arbitrary steering vector within the region Θ, and Θ_{m} stands for the mainlobe region.

Substituting (10) into (11), it yields,

$$\boldsymbol{y}_l^\dagger \boldsymbol{Z}_l \boldsymbol{y}_l = \xi, \tag{13}$$

where $\boldsymbol{y}_l \triangleq [1, \beta_l]^{\mathrm{T}} \in \mathbb{C}^2$, $\boldsymbol{Z}_l \in \mathbb{H}^{2\times 2}$ is expressed as

$$\begin{aligned} \boldsymbol{Z}_l &= \alpha_l^* [\boldsymbol{w}_\perp, \boldsymbol{w}_\parallel]^\dagger \boldsymbol{u}_l \boldsymbol{u}_l^\dagger \alpha_l [\boldsymbol{w}_\perp, \boldsymbol{w}_\parallel] \\ &= \alpha_l^* \alpha_l \begin{bmatrix} \boldsymbol{w}_\perp^\dagger \boldsymbol{u}_l \boldsymbol{u}_l^\dagger \boldsymbol{w}_\perp & \boldsymbol{w}_\perp^\dagger \boldsymbol{u}_l \boldsymbol{u}_l^\dagger \boldsymbol{w}_\parallel \\ \boldsymbol{w}_\parallel^\dagger \boldsymbol{u}_l \boldsymbol{u}_l^\dagger \boldsymbol{w}_\perp & \boldsymbol{w}_\parallel^\dagger \boldsymbol{u}_l \boldsymbol{u}_l^\dagger \boldsymbol{w}_\parallel \end{bmatrix} \\ &= \begin{bmatrix} \alpha_l^* \alpha_l \boldsymbol{w}_\perp^\dagger \boldsymbol{u}_l \boldsymbol{u}_l^\dagger \boldsymbol{w}_\perp & \alpha_l^* \alpha_l \boldsymbol{w}_\perp^\dagger \boldsymbol{u}_l \boldsymbol{u}_l^\dagger \boldsymbol{w}_\parallel \\ \alpha_l^* \alpha_l \boldsymbol{w}_\parallel^\dagger \boldsymbol{u}_l \boldsymbol{u}_l^\dagger \boldsymbol{w}_\perp & \alpha_l^* \alpha_l \boldsymbol{w}_\parallel^\dagger \boldsymbol{u}_l \boldsymbol{u}_l^\dagger \boldsymbol{w}_\parallel \end{bmatrix}. \end{aligned} \tag{14}$$

Substituting $\boldsymbol{w}_\perp^\dagger \boldsymbol{u}_l = 0$ into (14), then, Eq. (13) can be simplified as

$$\beta_l^2 \alpha_l^\dagger \alpha_l \boldsymbol{w}_\parallel^\dagger \boldsymbol{u}_l \boldsymbol{u}_l^\dagger \boldsymbol{w}_\parallel = \xi. \tag{15}$$

It will be shown in the following proposition that the solutions can be analytically solved.

Proposition 1. The solutions to (15) are obtained as

$$\breve{\beta}_l^1 = \frac{(a_3 + a_4) + \sqrt{\Delta}}{2\,(a_1 - a_2)}, \tag{16a}$$

$$\breve{\beta}_l^2 = \frac{(a_3 + a_4) - \sqrt{\Delta}}{2\,(a_1 - a_2)}, \tag{16b}$$

where $a_1 \triangleq \boldsymbol{w}_\parallel^\dagger \boldsymbol{u}_l \boldsymbol{u}_l^\dagger \boldsymbol{w}_\parallel$, $a_2 \triangleq \xi \boldsymbol{w}_\parallel^\dagger \boldsymbol{u}_0 \boldsymbol{u}_0^\dagger \boldsymbol{w}_\parallel$, $a_3 \triangleq \xi \boldsymbol{w}_\perp^\dagger \boldsymbol{u}_0 \boldsymbol{u}_0^\dagger \boldsymbol{w}_\parallel$, $a_4 \triangleq \xi \boldsymbol{w}_\parallel^\dagger \boldsymbol{u}_0 \boldsymbol{u}_0^\dagger \boldsymbol{w}_\perp$, $a_5 \triangleq \xi \boldsymbol{w}_\perp^\dagger \boldsymbol{u}_0 \boldsymbol{u}_0^\dagger \boldsymbol{w}_\perp$, and $\Delta = (a_3 + a_4)^2 + 4a_5(a_1 - a_2)$.

Proof. Please refer to Appendix B.

To maintain the responses of the beampattern according to the previous iterations maximally, a selection function is defined where the expression in the l-th iteration, $F_{\boldsymbol{w}_l, \boldsymbol{w}_{l-1}}(\beta_l)$ is written as

$$F_{\boldsymbol{w}_l, \boldsymbol{w}_{l-1}}(\beta_l) = \left\| \boldsymbol{P}\left(\boldsymbol{w}_{l-1}\right) \frac{\boldsymbol{w}_l}{\|\boldsymbol{w}_l\|_2} \right\|_2^2 = \left\| \frac{\boldsymbol{w}_{l-1} \boldsymbol{w}_{l-1}^\dagger \boldsymbol{w}_l}{\|\boldsymbol{w}_{l-1}\|_2 \|\boldsymbol{w}_l\|_2} \right\|_2^2. \tag{17}$$

In other words, it is supposed to minimize the difference between $B\left(\boldsymbol{u}_l \left| \boldsymbol{u}_0 \right.\right)$ and $B\left(\boldsymbol{u}_{l-1} \left| \boldsymbol{u}_0 \right.\right)$. Hence, β_l is picked from $\breve{\beta}_l^1$ and $\breve{\beta}_l^2$ by maximizing the similarity between the previous and the current iterations as

$$\beta_l = \mathop{\arg}_{\breve{\beta}_l^1, \breve{\beta}_l^2} \max \left(F_{\boldsymbol{w}_l, \boldsymbol{w}_{l-1}}\left(\breve{\beta}_l^1\right), F_{\boldsymbol{w}_l, \boldsymbol{w}_{l-1}}\left(\breve{\beta}_l^2\right) \right). \tag{18}$$

Hence, to evaluate the average difference between the response of the beampattern and the desired level ξ within the region Θ, a difference function is defined as

$$D_l = \begin{cases} \dfrac{1}{Q}\displaystyle\sum_{l=1}^{Q} \left| B\left(\boldsymbol{u}_l \left| \boldsymbol{u}_0\right.\right) - \xi \right|, \ \Theta = \Theta_{\mathrm{m}}, \\ \dfrac{1}{Q}\displaystyle\sum_{l=1}^{Q} \max\left(B\left(\boldsymbol{u}_l \left| \boldsymbol{u}_0\right.\right) - \xi, 0\right), \ \Theta \neq \Theta_{\mathrm{m}}, \end{cases} \tag{19}$$

where Q denotes the steering vectors within the region Θ, namely, the number of responses within the region Θ.

It is required that the iteration continues when $D_l > \varepsilon$. Notice that $\varepsilon > 0$ is a sufficiently small scalar. Thus, the ultimate weight vector is designed, and the proposed method is summarized in Algorithm 1. The main computational complexity lies in calculation of the projection matrix, which is $\mathcal{O}(M^4)$.

Algorithm 1 Weight vector orthogonal decomposition algorithm

Require: M, ε, σ_w^2, ξ, Θ, Θ_{m}, $D_1 > \varepsilon$, $\boldsymbol{u}_0$.
  Initialization: $l = 1$;
  while $D_l > \varepsilon$ **do**
    1. Determine $\boldsymbol{u}_l$ using Eq. (12);
    2. Calculate $\boldsymbol{Z}_l$ using Eq. (14), and determine $\breve{\beta}_l^{1}$ and $\breve{\beta}_l^{2}$ using Eq. (16);
    3. Substitute $\breve{\beta}_l^{1}$ and $\breve{\beta}_l^{2}$ into Eq. (17) to obtain β_l;
    4. Update $\boldsymbol{w}_l$ using Eq. (10);
    5. Calculate $B(\boldsymbol{u}_l|\boldsymbol{u}_0) = |\boldsymbol{w}_l^{\dagger}\boldsymbol{u}_l|^2$ and D_l according to Eq. (19);
    6. $l = l + 1$;
  end while
Ensure: the weight vector $\boldsymbol{w}_l$.

4 Multiple response control of transceive beampattern

4.1 Motivations and preliminary of oblique projection

From the previous discussions, a single response of the transceive beampattern of the FDA-MIMO radar can be accurately controlled by orthogonally decomposing the weight vector. However, in each iteration, only one specific response is adjusted, which means that only the current response $B(\boldsymbol{u}_l|\boldsymbol{u}_0)$ is precisely controlled. Moreover, when multiple responses are adjusted successively, the current response will have an influence on the previously-controlled responses. To circumvent these deficiencies and control multiple responses simultaneously, the oblique projection is utilized, where the preliminary is provided as follows.

Assume that $\boldsymbol{G} \in \mathbb{C}^{m\times p}$ and $\boldsymbol{H} \in \mathbb{C}^{m\times q}$ are matrices with full column rank. The subspaces spanned by the columns of $\boldsymbol{G}$ and $\boldsymbol{H}$, respectively denoted as $\langle \boldsymbol{G} \rangle$ and $\langle \boldsymbol{H} \rangle$, are disjointed, i.e., $p + q \leqslant m$. Different from the orthogonal projector[1)], oblique projections refer to projection matrices that are not orthogonal [38]. The orthogonal projection onto the linear subspace $\langle \boldsymbol{H}\ \boldsymbol{G} \rangle$ can be decomposed with $\boldsymbol{E}_{\boldsymbol{G}|\boldsymbol{H}} \in \mathbb{C}^{m\times m}$, and $\boldsymbol{E}_{\boldsymbol{H}|\boldsymbol{G}} \in \mathbb{C}^{m\times m}$ as

$$\boldsymbol{P}_{\langle \boldsymbol{H}\ \boldsymbol{G} \rangle} = \left(\boldsymbol{H}\ \ \boldsymbol{G} \right) \begin{pmatrix} \boldsymbol{H}^{\dagger}\boldsymbol{H} & \boldsymbol{H}^{\dagger}\boldsymbol{G} \\ \boldsymbol{G}^{\dagger}\boldsymbol{H} & \boldsymbol{G}^{\dagger}\boldsymbol{G} \end{pmatrix}^{-1} \begin{pmatrix} \boldsymbol{H}^{\dagger} \\ \boldsymbol{G}^{\dagger} \end{pmatrix} = \boldsymbol{E}_{\boldsymbol{G}|\boldsymbol{H}} + \boldsymbol{E}_{\boldsymbol{H}|\boldsymbol{G}}, \tag{20}$$

where the oblique projectors $\boldsymbol{E}_{\boldsymbol{G}|\boldsymbol{H}}$ and $\boldsymbol{E}_{\boldsymbol{H}|\boldsymbol{G}}$ are respectively defined as

$$\boldsymbol{E}_{\boldsymbol{G}|\boldsymbol{H}} = \left(\boldsymbol{G}\ \ \boldsymbol{0}_{m\times m} \right) \begin{pmatrix} \boldsymbol{H}^{\dagger}\boldsymbol{H} & \boldsymbol{H}^{\dagger}\boldsymbol{G} \\ \boldsymbol{G}^{\dagger}\boldsymbol{H} & \boldsymbol{G}^{\dagger}\boldsymbol{G} \end{pmatrix}^{-1} \begin{pmatrix} \boldsymbol{H}^{\dagger} \\ \boldsymbol{G}^{\dagger} \end{pmatrix} = \boldsymbol{G}\left(\boldsymbol{G}^{\dagger}\boldsymbol{P}_{\boldsymbol{H}}^{\perp}\boldsymbol{G}\right)\boldsymbol{G}^{\dagger}\boldsymbol{P}_{\boldsymbol{H}}^{\perp}, \tag{21a}$$

1) The orthogonal projector onto $\langle \boldsymbol{G} \rangle$ is constructed as $\boldsymbol{P}_{\boldsymbol{G}} = \boldsymbol{G}(\boldsymbol{G}^{\dagger}\boldsymbol{G})^{-1}\boldsymbol{G}^{\dagger} \in \mathbb{C}^{m\times m}$. The orthogonal projector onto the orthogonal complementary space of $\langle \boldsymbol{G} \rangle$ is $\boldsymbol{P}_{\boldsymbol{G}}^{\perp} = \boldsymbol{I}_{m\times m} - \boldsymbol{P}_{\boldsymbol{G}} \in \mathbb{C}^{m\times m}$. Similarly, $\boldsymbol{P}_{\boldsymbol{H}} = \boldsymbol{H}(\boldsymbol{H}^{\dagger}\boldsymbol{H})^{-1}\boldsymbol{H}^{\dagger} \in \mathbb{C}^{m\times m}$ and $\boldsymbol{P}_{\boldsymbol{H}}^{\perp} = \boldsymbol{I}_{m\times m} - \boldsymbol{P}_{\boldsymbol{H}} \in \mathbb{C}^{m\times m}$.

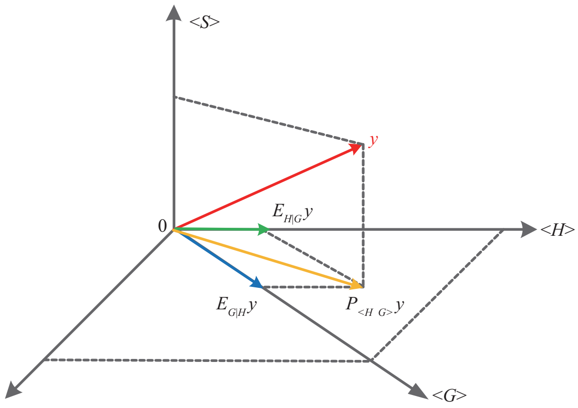

Figure 2 (Color online) Illustration of oblique projection.

$$\boldsymbol{E}_{\boldsymbol{H}|\boldsymbol{G}} = (\,\boldsymbol{0}_{m\times m}\ \ \boldsymbol{H}\,)\begin{pmatrix}\boldsymbol{H}^\dagger\boldsymbol{H} & \boldsymbol{H}^\dagger\boldsymbol{G}\\ \boldsymbol{G}^\dagger\boldsymbol{H} & \boldsymbol{S}^\dagger\boldsymbol{G}\end{pmatrix}^{-1}\begin{pmatrix}\boldsymbol{H}^\dagger\\ \boldsymbol{G}^\dagger\end{pmatrix} = \boldsymbol{H}\left(\boldsymbol{H}^\dagger\boldsymbol{P}_{\boldsymbol{G}}^{\perp}\boldsymbol{H}\right)\boldsymbol{H}^\dagger\boldsymbol{P}_{\boldsymbol{G}}^{\perp}. \tag{21b}$$

As shown in Figure 2, $\boldsymbol{E}_{\boldsymbol{G}|\boldsymbol{H}}$ projects vectors onto $\langle\boldsymbol{G}\rangle$ along the direction parallel to $\langle\boldsymbol{H}\rangle$, and $\boldsymbol{E}_{\boldsymbol{H}|\boldsymbol{G}}$ projects vectors onto $\langle\boldsymbol{H}\rangle$ along the direction parallel to $\langle\boldsymbol{G}\rangle$. To complete the null space, define $\boldsymbol{S}$ to span the perpendicular space to $\langle\boldsymbol{H}\ \boldsymbol{G}\rangle$. Since $\boldsymbol{P}_{\boldsymbol{G}}^{\perp}\boldsymbol{S} = \boldsymbol{S}$ and $\boldsymbol{G}^\dagger\boldsymbol{S} = \boldsymbol{0}_{m\times m}$, we have

$$\begin{aligned}\boldsymbol{E}_{\boldsymbol{G}|\boldsymbol{H}}\boldsymbol{S} &= \boldsymbol{G}\left(\boldsymbol{G}^\dagger\boldsymbol{P}_{\boldsymbol{H}}^{\perp}\boldsymbol{G}\right)\boldsymbol{G}^\dagger\boldsymbol{P}_{\boldsymbol{H}}^{\perp}\boldsymbol{S}\\ &= \boldsymbol{G}\left(\boldsymbol{G}^\dagger\boldsymbol{P}_{\boldsymbol{H}}^{\perp}\boldsymbol{G}\right)\boldsymbol{G}^\dagger\boldsymbol{S}\\ &= \boldsymbol{0}_{m\times m}.\end{aligned} \tag{22}$$

According to (22), the range and the null space of $\boldsymbol{E}_{\boldsymbol{G}|\boldsymbol{H}}$ are $\langle\boldsymbol{G}\rangle$ and $\langle\boldsymbol{H}\ \boldsymbol{S}\rangle$, respectively. It is seen that $\langle\boldsymbol{S}\rangle$ is also in the null space of $\boldsymbol{E}_{\boldsymbol{G}|\boldsymbol{H}}$. As all available dimensions have been accounted, the null space of $\boldsymbol{E}_{\boldsymbol{G}|\boldsymbol{H}}$ is $\langle\boldsymbol{H}\ \boldsymbol{S}\rangle$. Hence, it can be verified that $\boldsymbol{E}_{\boldsymbol{G}|\boldsymbol{H}}\boldsymbol{G} = \boldsymbol{G}$, $\boldsymbol{E}_{\boldsymbol{G}|\boldsymbol{H}}\boldsymbol{H} = \boldsymbol{0}_{m\times m}$, $\boldsymbol{E}_{\boldsymbol{H}|\boldsymbol{G}}\boldsymbol{H} = \boldsymbol{H}$, and $\boldsymbol{E}_{\boldsymbol{H}|\boldsymbol{G}}\boldsymbol{G} = \boldsymbol{0}_{m\times m}$.

4.2 MRCOP algorithms to control multiple responses simultaneously

Consider a region set $\{\Theta_k\}_{k=1}^K$ and its corresponding predefined response set $\{\xi_k\}_{k=1}^K$. To control multiple regions simultaneously, a feasible way is to adjust K points from their corresponding regions concurrently, i.e., the C-MRCOP method. Define a response control matrix by collecting all steering vectors from K regions as

$$\tilde{\boldsymbol{A}} \triangleq [\boldsymbol{u}_0, \boldsymbol{u}_{l,1}, \ldots, \boldsymbol{u}_{l,K}] \in \mathbb{C}^{M^2\times(K+1)}, \tag{23}$$

where $\boldsymbol{u}_{l,k} \in \mathbb{C}^{M^2}$ denotes the steering vector of the response in the k-th region which is supposed to be adjusted in the l-th iteration. Removing $\boldsymbol{u}_{l,k}$ and $\boldsymbol{u}_0$ from $\tilde{\boldsymbol{A}}$ respectively, the matrices containing the surplus steering vectors are defined as

$$\tilde{\boldsymbol{A}}_{k-} \triangleq [\boldsymbol{u}_0, \boldsymbol{u}_{l,1}, \ldots, \boldsymbol{u}_{l,k-1}, \boldsymbol{u}_{l,k+1}, \ldots, \boldsymbol{u}_{l,K}] \in \mathbb{C}^{M^2\times K}, \tag{24a}$$

$$\tilde{\boldsymbol{A}}_{0-} \triangleq [\boldsymbol{u}_{l,1}, \boldsymbol{u}_{l,2}, \ldots, \boldsymbol{u}_{l,K}] \in \mathbb{C}^{M^2\times K}. \tag{24b}$$

Subsequently, oblique projectors based on (24) are defined as

$$\boldsymbol{E}_{k|\tilde{\boldsymbol{A}}_{k-}} \triangleq \boldsymbol{u}_{l,k}\left(\boldsymbol{u}_{l,k}^\dagger\boldsymbol{P}_{\tilde{\boldsymbol{A}}_{k-}}^{\perp}\boldsymbol{u}_{l,k}\right)^{-1}\boldsymbol{u}_{l,k}^\dagger\boldsymbol{P}_{\tilde{\boldsymbol{A}}_{k-}}^{\perp} \in \mathbb{C}^{M^2\times M^2},\quad k = 1, 2, \ldots, K, \tag{25a}$$

$$\boldsymbol{E}_{\tilde{\boldsymbol{A}}_{0-}|0} \triangleq \tilde{\boldsymbol{A}}_{0-}\left(\tilde{\boldsymbol{A}}_{0-}^\dagger\boldsymbol{P}_{\boldsymbol{u}_0}^{\perp}\tilde{\boldsymbol{A}}_{0-}\right)^{-1}\tilde{\boldsymbol{A}}_{0-}^\dagger\boldsymbol{P}_{\boldsymbol{u}_0}^{\perp} \in \mathbb{C}^{M^2\times M^2}. \tag{25b}$$

Moreover, the projections onto $\boldsymbol{u}_0$ are obtained as

$$\boldsymbol{E}_{k|\tilde{\boldsymbol{A}}_{k-}}\boldsymbol{u}_0 = \boldsymbol{0}_{M^2\times 1},\quad k = 1, 2, \ldots, K, \tag{26a}$$

$$\boldsymbol{E}_{\tilde{\boldsymbol{A}}_{0-}|0}\boldsymbol{u}_0 = \boldsymbol{0}_{M^2\times 1}. \tag{26b}$$

In addition, according to the properties of the oblique projection, for a steering vector from an arbitrary region, i.e., $\boldsymbol{u}_{l,i}$, $k, i = 1, \ldots, K$, it satisfies

$$\boldsymbol{E}_{k|\tilde{\boldsymbol{A}}_{k-}} \boldsymbol{u}_{l,i} = \begin{cases} \boldsymbol{u}_{l,i}, & i = k, \\ \boldsymbol{0}_{M\times 1}, & i \neq k, \end{cases} \tag{27a}$$

$$\boldsymbol{E}_{\tilde{\boldsymbol{A}}_{0-}|0} \boldsymbol{u}_{l,i} = \boldsymbol{u}_{l,i}. \tag{27b}$$

Furthermore, for the k-th region in the l-th iteration, we can construct a filtering matrix $\boldsymbol{T}_{l,k} \in \mathbb{C}^{M^2\times M^2}$ which passes the $\boldsymbol{u}_{l,k}$ and blocks the components from other regions. The final weight vector is obtained by filtering sub-weight vectors from K regions using the filtering matrix $\boldsymbol{T}_{l,k}$, which is expressed as

$$\breve{\boldsymbol{w}}_l = \sum_{k=1}^{K} \boldsymbol{T}_{l,k} \boldsymbol{w}_{l,k}, \tag{28}$$

where $\boldsymbol{w}_{l,k} \in \mathbb{C}^{M^2}$ denotes the weight vector, obtained using Algorithm 1, which controls the response of the k-th region in the l-th iteration. In particular, the formulation of $\boldsymbol{T}_{l,k}$ in the l-th iteration is expressed as follows:

$$\begin{aligned} &\boldsymbol{T}_{l,k} = \alpha_k \boldsymbol{I}_{M^2} + \beta_k \boldsymbol{E}^{\dagger}_{\tilde{\boldsymbol{A}}_{0-}|0} + \gamma_l \boldsymbol{E}^{\dagger}_{k|\tilde{\boldsymbol{A}}_{k-}}, \\ &\text{s.t.} \begin{cases} \breve{\boldsymbol{w}}_l^{\dagger} \boldsymbol{u}_0 = \displaystyle\sum_{k=1}^{K} \boldsymbol{w}_{l,k}^{\dagger} \boldsymbol{T}_{l,k}^{\dagger} \boldsymbol{u}_0 = 1, \\ \breve{\boldsymbol{w}}_l^{\dagger} \boldsymbol{u}_{l,k} = \displaystyle\sum_{i=1}^{K} \boldsymbol{w}_{l,i}^{\dagger} \boldsymbol{T}_{l,k}^{\dagger} \boldsymbol{u}_{l,k} = \boldsymbol{w}_{l,k}^{\dagger} \boldsymbol{u}_{l,k}, \quad k = 1, 2, \ldots, K, \end{cases} \end{aligned} \tag{29}$$

where $\alpha_k \in \mathbb{R}^1$, $\beta_k \in \mathbb{R}^1$, and $\gamma_k \in \mathbb{R}^1$ are the coefficients to be determined. Notice that $\boldsymbol{T}_{l,k}$ is identical for different iterations. Recall that $\boldsymbol{w}_{l,k}^{\dagger} \boldsymbol{u}_0 = 1$. By substituting (28) into (29), the coefficients in (29) are calculated as

$$\sum_{k=1}^{K} \alpha_k = 1, \ \alpha_k + \beta_k = 0, \ \gamma_l = 1. \tag{30}$$

For $k = 1, 2, \ldots, K$, it is verified that

$$\begin{aligned} \breve{\boldsymbol{w}}_l^{\dagger} \boldsymbol{u}_{l,k} &= \sum_{i=1}^{K} \boldsymbol{w}_{l,i}^{\dagger} \big(\alpha_i \boldsymbol{I}_{M^2} + \beta_i \boldsymbol{E}_{\tilde{\boldsymbol{A}}_{0-}|0}\big) \boldsymbol{u}_{l,k} \\ &\quad + \gamma_l \sum_{i=1}^{K} \boldsymbol{w}_{l,i}^{\dagger} \boldsymbol{E}^{\dagger}_{i|\tilde{\boldsymbol{A}}_{i-}} \boldsymbol{u}_{l,k} \\ &\overset{i=k}{=} \sum_{k=1}^{K} \boldsymbol{w}_{l,k}^{\dagger} (\alpha_k + \beta_k) \boldsymbol{u}_{l,k} + \gamma_l \boldsymbol{w}_{l,k}^{\dagger} \boldsymbol{u}_{l,k} \\ &= \gamma_l \boldsymbol{w}_{l,k}^{\dagger} \boldsymbol{u}_{l,k} = \boldsymbol{w}_{l,k}^{\dagger} \boldsymbol{u}_{l,k}, \end{aligned} \tag{31a}$$

$$\begin{aligned} \breve{\boldsymbol{w}}_l^{\dagger} \boldsymbol{u}_0 &= \sum_{k=1}^{K} \boldsymbol{w}_{l,k}^{\dagger} (\alpha_k \boldsymbol{u}_0 + \beta_k \boldsymbol{0}_{M^2\times 1} + \gamma_k \boldsymbol{0}_{M^2\times 1}) \\ &= \sum_{k=1}^{K} \alpha_k \boldsymbol{w}_{l,k}^{\dagger} \boldsymbol{u}_0 = 1. \end{aligned} \tag{31b}$$

Define $D_{k,l}$ as the average difference between the response of the beampattern and ξ_k within the region Θ_k. For non-mainlobe and mainlobe regions, it can be respectively expressed as

$$D_{k,l} = \begin{cases} \dfrac{1}{Q_k} \displaystyle\sum_{l=1}^{Q_k} \max |B(\boldsymbol{u}_{l,k} | \boldsymbol{u}_0) - \xi_k|, & \Theta_k = \Theta_{\mathrm{m}}, \\ \dfrac{1}{Q_k} \displaystyle\sum_{l=1}^{Q_k} \max (B(\boldsymbol{u}_{l,k} | \boldsymbol{u}_0) - \xi_k, 0), & \Theta_k \neq \Theta_{\mathrm{m}}, \end{cases} \tag{32}$$

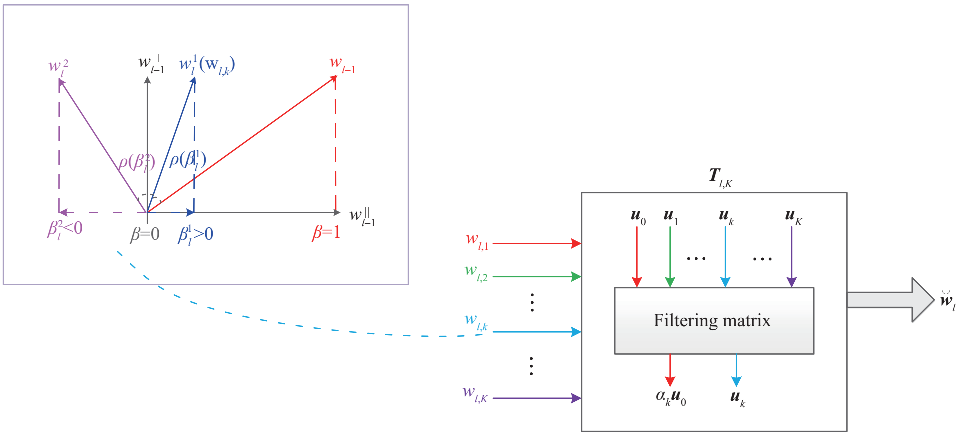

Figure 3 (Color online) The proposed C-MRCOP method.

where $B(\boldsymbol{u}_{l,k}|\boldsymbol{u}_0) = |\breve{\boldsymbol{w}}_l^\dagger \boldsymbol{u}_{l,k}|^2$, and Q_k denotes the number of responses within Θ_k.

Consider that the response adjusted in the current iteration will influence other responses within Θ_k, hence, in order to avoid excessive control, if $D_{k,l} < \varepsilon$ is satisfied for Θ_k, $\boldsymbol{u}_{k,q}$ is supposed to be omitted.

Define a diagonal selecting matrix $\boldsymbol{S}_l \in \mathbb{C}^{M^2 \times M^2}$. The matrix consists of a sequence of 1 and 0, where 0 represents the indexes of regions satisfying $D_{k,l} < \varepsilon$, and 1 denotes the remaining regions. The updated response control matrix is written as

$$\bar{\boldsymbol{A}} = \tilde{\boldsymbol{A}} \cdot \boldsymbol{S}_l = [\boldsymbol{u}_0, \boldsymbol{u}_{l,1}, \ldots, \boldsymbol{u}_{l,\tilde{K}}] \in \mathbb{C}^{M^2 \times \tilde{K}}, \tag{33}$$

where $\tilde{K} \leqslant K$ denotes the actual number of regions which need to be controlled.

Hence, $\breve{\boldsymbol{w}}_l$ fulfills the task of concurrently controlling multiple responses. Algorithm 2 is presented to summarize the proposed C-MRCOP method. Figure 3 demonstrates the proposed C-MRCOP method.

Algorithm 2 C-MRCOP algorithm

Require: M, K, ε, σ_w^2, $\{\xi_k\}_{k=1}^K$, $\{\Theta_k\}_{k=1}^K$, Θ_{m}, $\boldsymbol{u}_0$, Q, $\boldsymbol{w}_{0,k} = \boldsymbol{u}_0$.

Initialization: $l = 1$.

1. Calculate $D_{k,1}$ according to Eq. (32), and determine the maximum value $\max_k D_{k,1}$;

while $\max_k D_{k,l} > \varepsilon$ **do**

2. Calculate $D_{k,l}$ using Eq. (32) to determine the diagonal selecting matrix $\boldsymbol{S}_l$;
3. Obtain the response control matrix $\bar{\boldsymbol{A}}$ according to Eq. (33) and $\tilde{K}$;
4. Determine $\{\boldsymbol{w}_{l,k}\}_{k=1}^{\tilde{K}}$ from $\tilde{K}$ regions according to Algorithm 1 with $\boldsymbol{w}_{l.k} = \alpha_g(\boldsymbol{w}_{l-1,k}^{\perp} + \beta_l \boldsymbol{w}_{l-1,k}^{\parallel})$;
5. Calculate $\{\boldsymbol{T}_{l,k}\}_{k=1}^{\tilde{K}}$ for $\tilde{K}$ regions using Eq. (29);
6. Construct $\breve{\boldsymbol{w}}_l = \sum_{k=1}^{\tilde{K}} \boldsymbol{T}_{l,k} \boldsymbol{w}_{l,k}$ according to Eq. (28);
7. Obtain the current beampattern $B(\boldsymbol{u}_{l,k}|\boldsymbol{u}_0) = |\breve{\boldsymbol{w}}_l^\dagger \boldsymbol{u}_{l,k}|^2$ and $D_{k,l}$ according to Eq. (32);
8. $l = l + 1$;
9. Denote $\boldsymbol{w}_{l-1,k} = \breve{\boldsymbol{w}}_l$;

end while

Ensure: the final weight vector $\breve{\boldsymbol{w}}_l$.

Moreover, another way to control multiple regions successively, termed as the S-MRCOP method, is proposed. This method is performed by successively controlling K regions. In the S-MRCOP algorithm, G_k is the number of response points to be controlled within the k-th region, and we have a set $\{G_k\}_{k=1}^K$. For the k-th region, the matrices in (24) are defined as

$$\tilde{\boldsymbol{A}}_{g-} \triangleq [\boldsymbol{u}_0, \boldsymbol{u}_{l,1}, \ldots, \boldsymbol{u}_{l,g-1}, \boldsymbol{u}_{l,g+1}, \ldots, \boldsymbol{u}_{l,G_k}] \in \mathbb{C}^{M^2 \times G_k}, \quad g = 1, 2, \ldots, G_k, \tag{34a}$$

$$\tilde{\boldsymbol{A}}_{0-} \triangleq [\boldsymbol{u}_{l,1}, \boldsymbol{u}_{l,2}, \ldots, \boldsymbol{u}_{l,G_k}] \in \mathbb{C}^{M \times G_k}. \tag{34b}$$

For each point $\boldsymbol{u}_{g,l} \in \mathbb{C}^{M^2}$ in the k-th region, the sub-weight vector $\boldsymbol{w}_{l,g} = \alpha_g(\boldsymbol{w}_{l-1,g}^{\perp} + \beta_l \boldsymbol{w}_{l-1,g}^{\parallel}) \in \mathbb{C}^{M^2}$ is calculated using Algorithm 1 with $\alpha_g = \frac{1}{\boldsymbol{u}_0^\dagger \boldsymbol{w}_{l-1,g}^{\perp} + \beta_l \boldsymbol{u}_0^\dagger \boldsymbol{w}_{l-1,g}^{\parallel}}$.

Subsequently, the ultimate weight vector in the k-th region is formulated using oblique projection, which is expressed as

$$\breve{\boldsymbol{w}}_k = \sum_{g=1}^{G_k} \boldsymbol{T}_{g,l}\boldsymbol{w}_{l,g}, \tag{35}$$

where $\boldsymbol{T}_{l,g} \in \mathbb{C}^{M^2\times M^2}$ is expressed as

$$\boldsymbol{T}_{l,g} = \alpha_k \boldsymbol{I}_M + \beta_k \boldsymbol{E}^{\dagger}_{\tilde{\boldsymbol{A}}_{0-}|0} + \gamma_k \boldsymbol{E}^{\dagger}_{g|\tilde{\boldsymbol{A}}_{g-}}, \tag{36}$$

where $\boldsymbol{E}_{g|\tilde{\boldsymbol{A}}_{g-}} \triangleq \boldsymbol{u}_{l,g}(\boldsymbol{u}^{\dagger}_{l,g}\boldsymbol{P}^{\perp}_{\tilde{\boldsymbol{A}}_{k-}}\boldsymbol{u}_{l,g})^{-1}\boldsymbol{u}^{\dagger}_{l,g}\boldsymbol{P}^{\perp}_{\tilde{\boldsymbol{A}}_{g-}}$. Hence, the response requirement for G_k responses of the beampattern is satisfied.

We start the algorithm from the first region. Iterations are performed to update the weight vector successively. To retain the response results maximally from the previous iteration , the optimal weight vector obtained in the $(k-1)$-th region is assigned as the previous weight vector in the k-th iteration. Algorithm 3 is presented to summarize the proposed S-MRCOP method. The S-MRCOP algorithm shares the advantage of easy operation. However, the number of controlled points within each region is limited to DOFs. Besides, the selection of $\boldsymbol{u}_{l,g}$ will influence the performance, and the currently-controlled responses may have influence on the previously-controlled region.

Algorithm 3 S-MRCOP algorithm

Require: M, K, $\{G_k\}_{k=1}^K$, ε, σ_w^2, $\{\xi_k\}_{k=1}^K$, $\{\Theta_k\}_{k=1}^K$, $\Theta_{\rm m}$, $\boldsymbol{u}_0$, $\boldsymbol{w}_{0,g} = \boldsymbol{u}_0$, Q.
  Initialization: $l = 1$.
  for $k = 1, 2, \ldots, K$ **do**
    1. Determine $\{\boldsymbol{w}_{l,g}\}_{g=1}^{G_k}$ for G_k responses in the k-th region according to Algorithm 1 with $\boldsymbol{w}_{l,g} = \alpha_g(\boldsymbol{w}^{\perp}_{l-1,g} + \beta_l \boldsymbol{w}^{\parallel}_{l-1,g})$;
    2. Calculate $\{\boldsymbol{T}_{l,g}\}_{g=1}^{G_k}$ for G_k points using Eq. (29);
    3. Construct $\breve{\boldsymbol{w}}_k = \sum_{g=1}^{G_k} \boldsymbol{T}_{g,l}\boldsymbol{w}_{l,g}$ according to Eq. (35);
    4. Denote $\boldsymbol{w}_{l-1,g} = \breve{\boldsymbol{w}}_k$;
  end for
Ensure: the final weight vector $\breve{\boldsymbol{w}}_K$.

4.3 Performance analysis

It is obvious that the resulting final weight vector $\breve{\boldsymbol{w}}_l$ fulfills the task of concurrently controlling multiple responses. On the one hand, $\breve{\boldsymbol{w}}_l$ keeps the responses adjusted in the previous iteration using orthogonal decomposition of the weight vector. On the other hand, based on the oblique projection, multiple responses are controlled simultaneously using the filtering matrix $\boldsymbol{T}_{l,k}$ in each iteration. Actually, for the k-th region, the designed filtering matrix 'selects' the sub-weight vector corresponding to the k-th region, while it 'blocks' the sub-weight vectors from other regions. Moreover, the matrix $\boldsymbol{T}_{l,k}$ keeps the previously-controlled responses. In other words, the response for each region can be controlled separately because only the response corresponding to the current iteration is adjusted. Closed-form expressions of the ultimate weight vectors are obtained using either the C-MRCOP or S-MRCOP algorithms. The main computational complexity lies in the calculations of oblique projectors $\boldsymbol{E}_{k|\tilde{\boldsymbol{A}}_{k-}}$ and $\boldsymbol{E}_{\tilde{\boldsymbol{A}}_{0-}|0}$. Particularly, the computational complexity for each oblique projector is $\mathcal{O}(M^6)$. As a result, the computational complexities for both the C-MRCOP and S-MRCOP are $\mathcal{O}(M^6)$.

5 Numerical and measured results

In this section, numerical and measured results are performed to evaluate the beampattern control methods in FDA-MIMO radar. The proposed algorithms are firstly applied to the one-dimensional (1-D) slice of the equivalent transmit beampattern in the equivalent angle domain, which is performed in the receiver side. Subsequently, experimental results with real antenna data are shown to demonstrate the performance of controlling the range-angle-dependent 2-D transceive beampattern in the joint range-angle domain. Simulation parameters are listed in Table 1.

Table 1 Simulation parameters of FDA-MIMO

Parameter	Value
Transmit elements	16
receive elements	16
Wavelength	0.0187 m
reference carrier frequency	10 GHz
Bandwidth	2 MHz
Frequency increment	3750 Hz
Range of the target	10 km
Angle of the target	30°

5.1 Equivalent transmit beampattern with simulated results

In this subsection, the proposed algorithms are implemented to control the 1-D transmit beampattern in the equivalent angle domain with the FDA-MIMO radar. Notice that, owing to the frequency increment introduced in the transmit array, an offset $-\Delta f\frac{2R_0}{c}$ is introduced. In this respect, the mainlobe of the equivalent transmit beampattern of the FDA-MIMO radar is different from that of the MIMO radar. For instance, in FDA-MIMO radar, the corresponding transmit spatial frequency of a target, which is located at $\theta_0 = 30°$, is calculated as $f_{\mathrm{T}}^s = -\Delta f\frac{2R_0}{c} + \frac{d}{\lambda_0}\sin(\theta_0) = 0$ [37], hence, the equivalent angle is defined as $\tilde{\theta}_0 = \arcsin(f_{\mathrm{T}}^s\frac{\lambda_0}{d}) = 0°$.

Figure 4(a) demonstrates the 1-D plot of the equivalent transmit beampattern with two controlled nulls. Assume that the predefined depths are $\xi_1 = -50$ dB and $\xi_2 = -55$ dB, respectively. The regions in the angle domain are assumed to be $[-50°, -40°]$ and $[30°, 40°]$, respectively. It is observed that the beampattern with two broadened notches is achieved with the proposed C-MRCOP and S-MRCOP methods. Notice that we have $G_1 = 4$ and $G_2 = 5$. However, the sidelobes with the S-MRCOP method are not a desired result, because the currently-controlled response will influence the previously-controlled ones. Moreover, the LCSS [39] and LCMV [40] methods, which are used for conventional array radars, are compared. Although the LCSS and LCMV methods can obtain a beampattern with broadened and deep notches, the response cannot be controlled. In contrast, the beampattern with broadened notches is obtained with the C-MRCOP method. In Figure 4(b), the equivalent transmit beampatterns are plotted versus different numbers of iterations, where $\varepsilon = 0.01$. It can be seen that after 80 steps, the synthesized beampattern is close to the desired one, and a satisfactory beampattern is obtained after 150 iterations.

Figure 4(c) demonstrates the 1-D equivalent transmit beampattern with two broadened notches and low sidelobes. The desired sidelobe level is -20 dB, and the depths of notches are -45 and -40 dB, respectively. In order to simplify the synthesis procedure, we employ the Chebyshev weight with a -20 dB of sidelobe attenuation as the initial weight vector. For comparison, the resulting beampatterns using the A^{2}RC [32], WORD [33], and the artificial interferences based method [18] are also displayed. The result of the S-MRCOP method is omitted, because the performance of this approach degrades. It is due to the fact that the currently-controlled response will influence the previously-controlled ones when multiple responses are controlled successively. It can be seen that the C-MRCOP method has a satisfactory beampattern. The A^{2}RC and WORD methods can also generate a beampattern with broadened nulls and low sidelobes. The beampattern with a flat-top mainlobe within $[-8°, 8°]$, two broadened notches, and low sidelobes are obtained in Figure 4(d). The sidelobe level is set as -25 dB, and depths for two null regions are -55 and -50 dB, respectively. It is shown that a desired beampattern with controlled responses is synthesized using the C-MRCOP method. Moreover, it is also seen from the enlarged figures that a more precious beampattern with the minimum fluctuation in the mainlobe is obtained using the C-MRCOP method. The corresponding weight vectors obtained with C-MRCOP are listed in Table 2. Moreover, the SDR [23], A^{2}RC [32], and WORD [33] methods are implemented for comparison. Note that, the method using artificial interferences in [18] fials to control the mainlobe. Terms, including runtimes, average difference, and iteration numbers, are listed in Table 3. It is seen from Table 3 that the C-MRCOP converges faster with reduced runtimes and less iteration numbers compared with the other methods. The runtimes of WORD, A^{2}RC, artificial interferences based, and C-MRCOP methods are 2.89, 2.91, 0.29, and 0.61 s, respectively. Furthermore, the average maximum difference for multiple regions between the resultant beampattern and the desired response is smaller. Besides, methods such as the WORD and A^{2}RC update the weight vector in a point-by-point manner, which fail to control multiple points simultaneously. Therefore, the C-MRCOP method outperforms the other methods in the

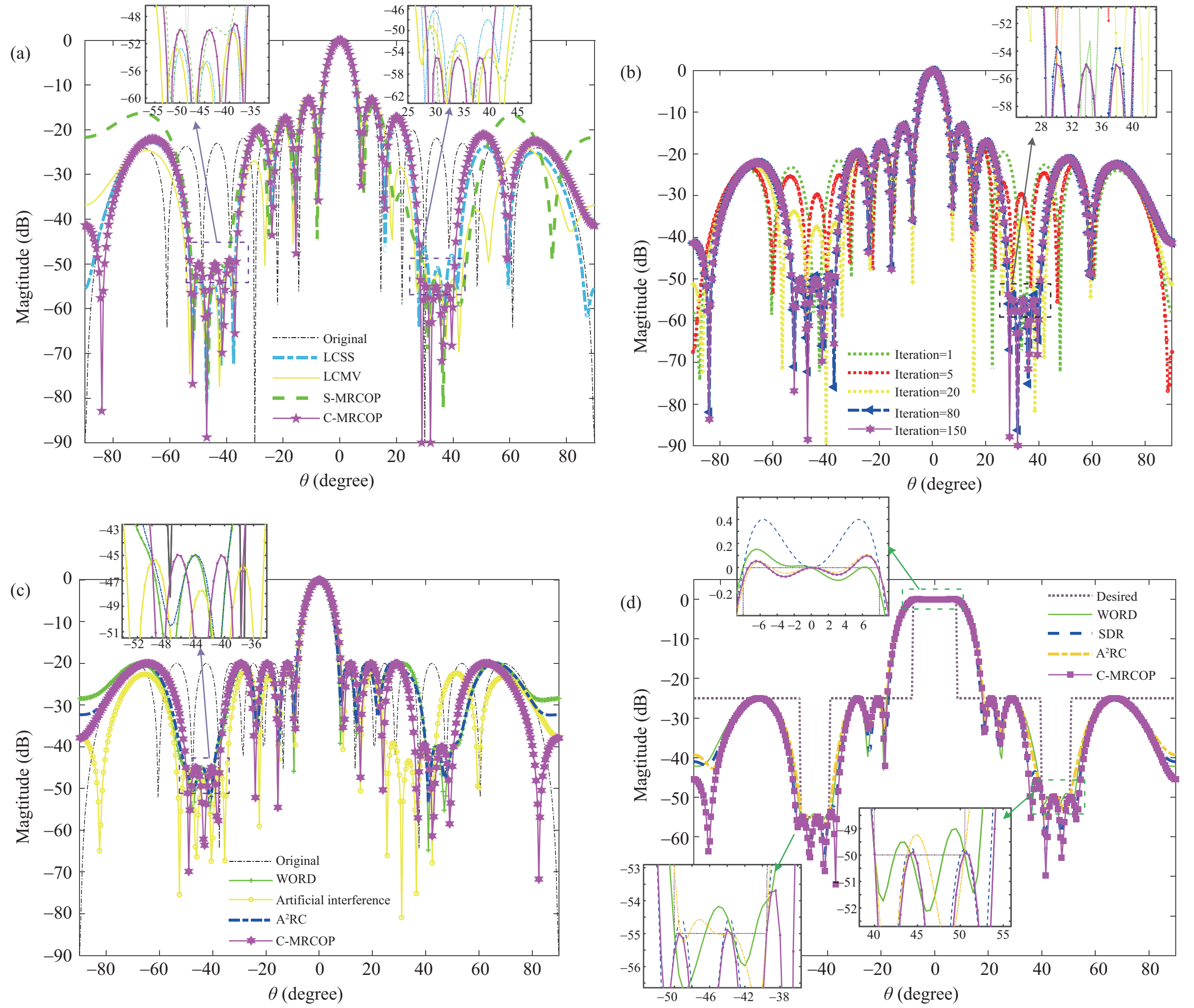

Figure 4 (Color online) Equivalent transmit beampattern in the transmit spatial domain. (a) Beampattern with two accurately controlled nulls; (b) beampattern versus number of iterations; (c) beampattern with two accurately controlled notches and low sidelobes; (d) beampattern with a flat-top mainlobe, two accurately controlled notches and low sidelobes.

Table 2 Weight vectors obtained with C-MRCOP

Element	Weight vector	Element	Weight vector
1	$0.0268e^{+j2.0332}$	9	$0.2177e^{-j0.5228}$
2	$0.0487e^{+j1.8918}$	10	$0.1706e^{-j0.4363}$
3	$0.0697e^{+j1.7327}$	11	$0.1176e^{-j0.4363}$
4	$0.0538e^{+j1.0652}$	12	$0.0644e^{+j0.3527}$
5	$0.0640e^{+j0.3328}$	13	$0.0555e^{+j1.0865}$
6	$0.1151e^{-j0.2575}$	14	$0.0701e^{+j1.7569}$
7	$0.1677e^{-j0.4341}$	15	$0.0494e^{+j1.8931}$
8	$0.2160e^{-j0.5196}$	16	$0.0266e^{+j2.1132}$

Table 3 Comparisons of different methods

Method	Runtime (s)	Average difference (dB)	Iteration number
C-MRCOP	1.01	0.1026	200
SDR	78.16	0.2649	8
WORD	3.47	0.3895	2000
A^2RC	3.37	0.4904	2000

following aspects: (1) less processing time; (2) lower sidelobes; (3) a flatter mainlobe.

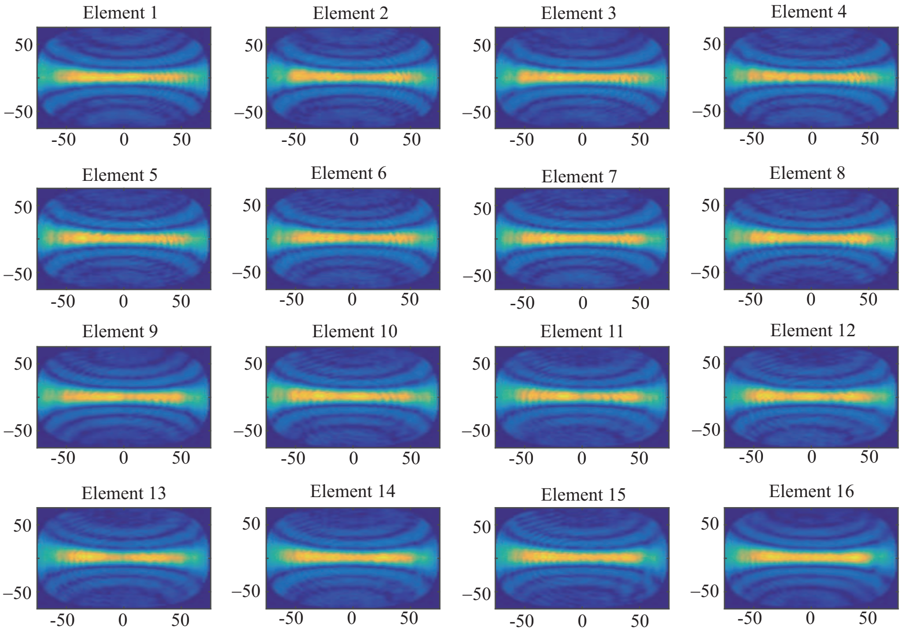

Figure 5 (Color online) Element response of 16 elements.

Table 4 Actual positions of the antenna elements

	Elemen1	Elemen2	Elemen3	Elemen4	Elemen5	Elemen6	Elemen7	Elemen8
x-axis (mm)	2.2149	2.7459	−1.3841	0.9269	−1.2631	−0.6691	−0.9791	0.0519
y-axis (mm)	−70.1975	−61.2545	−52.5485	−42.1855	−32.2045	−23.0975	−13.8915	−4.5835
z-axis (mm)	−0.0690	2.3700	3.2260	3.1760	2.1360	3.4760	2.6850	1.7530
	Elemen9	Elemen10	Elemen11	Elemen12	Elemen13	Elemen14	Elemen15	Elemen16
x-axis (mm)	−0.7341	1.0639	0.4679	0.3639	−1.9191	−0.4341	−0.3681	−0.0841
y-axis (mm)	4.7365	14.2225	22.6145	33.2375	42.6655	51.7785	61.1615	71.0435
z-axis (mm)	1.9650	1.3300	1.8000	2.5380	3.3230	0.5070	1.0560	1.1640

5.2 Range-angle-dependent transceive beampattern with measured results

In this subsection, measured results are provided to verify the effectiveness of the proposed methods. In specific, the antenna measurement is carried out, where an FDA with 16 antenna elements is employed. In this respect, the practical antenna element pattern, i.e., $\boldsymbol{g}(\theta_0)$, is considered in the beampattern design, where the element responses for 16 elements are presented in Figure 5, and the actual positions of the antenna elements in the descartes coordinate system are listed in Table 4, where the phase center is the middle of the 8th and 9th elements.

Figure 6 compares the original 2-D transceive beampatterns between the conventional MIMO radar and FDA-MIMO radar, where the target is located at $R_0 = 10$ km and $\theta_0 = 0°$. Different from the conventional MIMO radar, the transceive beampattern of FDA-MIMO radar is range-angle-dependent, while the transceive beampattern is only angle-dependent for conventional MIMO radar.

Figure 7 demonstrates the designed 2-D range-angle-dependent transceive beampattern in FDA-MIMO radar. Assume that the null depth for both two null regions is −45 dB, and the sidelobe level is −20 dB. Figure inspirations in Figure 7(a) highlights the effectiveness of the proposed methods in forming a range-angle-dependent transceive beampattern with a desired shape, where two rectangular null regions and a flat-top mainlobe are obtained. The range and angle regions of the mainlobe are assumed as $[-7°, 7°]$ and $[9, 11]$ km, respectively. As for the first null region, the range and angle regions are assumed as $[-7°, 7°]$ and $[25, 30]$ km, respectively. The range and angle regions of the second null region are assumed as $[-50°, -40°]$ and $[9, 11]$ km, respectively. As shown by the 1-D range-dependent beampatterns at $\theta_0 = 0°$ in Figure 7(b), the measured results coincide with the simulated ones, which verifies the effectiveness of the proposed method. Figure 7(c) demonstrates the 1-D angle-dependent beampatterns at $R_0 = 10$ km. Notice that the null depth cannot be as low as desired due to system errors with measured data.

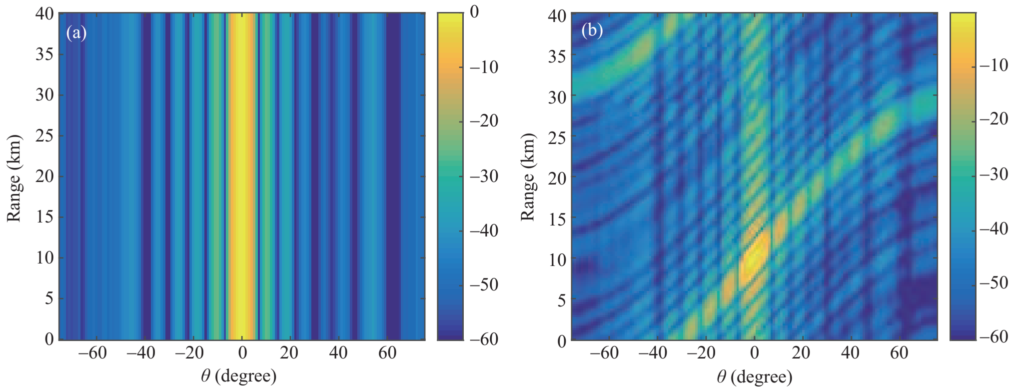

Figure 6 (Color online) Comparison of original transceive beampatterns. (a) Conventional MIMO radar; (b) FDA-MIMO radar.

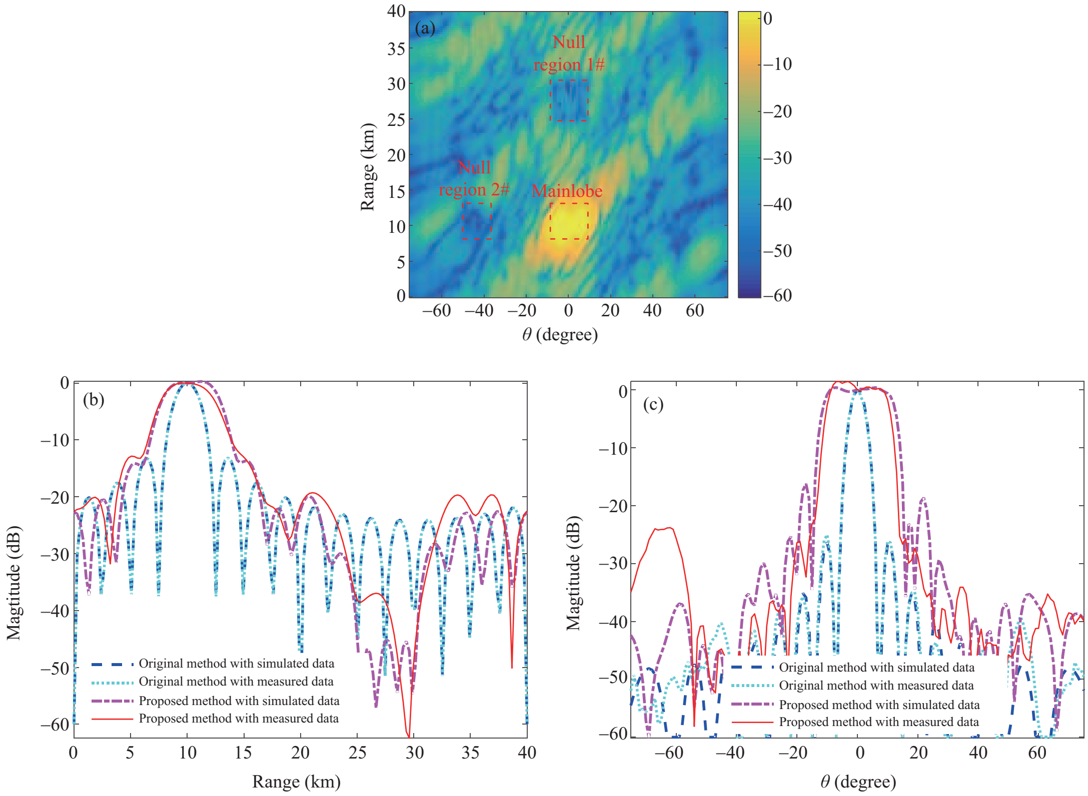

Figure 7 (Color online) Designed range-angle-dependent transceive beampatterns with measured data. (a) Resultant 2-D beampattern; (b) 1-D range-dependent beampattern at $\theta_0 = 0°$; (c) 1-D angle-dependent beampattern at $R_0 = 10$ Km.

5.3 Application of interference mitigation

In this subsection, the mitigation of mainlobe interferences in the dynamic environment is evaluated, where the interferences are regarded as point scatterers. As considered in [37], the interferences can be suppressed by nulling at the range-angle-dependent beampattern. However, when time-varying interferences are considered, the mismatches exist in both mainlobe and nulling angles, leading to a failure of interference suppression. In this respect, using the proposed C-MRCOP method, the received echoes of the target and interferences can be suppressed through a 2-D data-independent beamformer, where the weight vector is obtained by using the output of Algorithm 2, that is

$$\boldsymbol{w}_{\mathrm{C-MRCOP}} = \breve{\boldsymbol{w}}_l. \tag{37}$$

Figure 8 investigates the interference suppression performance, where two interferences exist. The the range and angle of the first interference is $\theta_{j1} = -45°$ and $R_{j1} = 10$ km, respectively. For the second

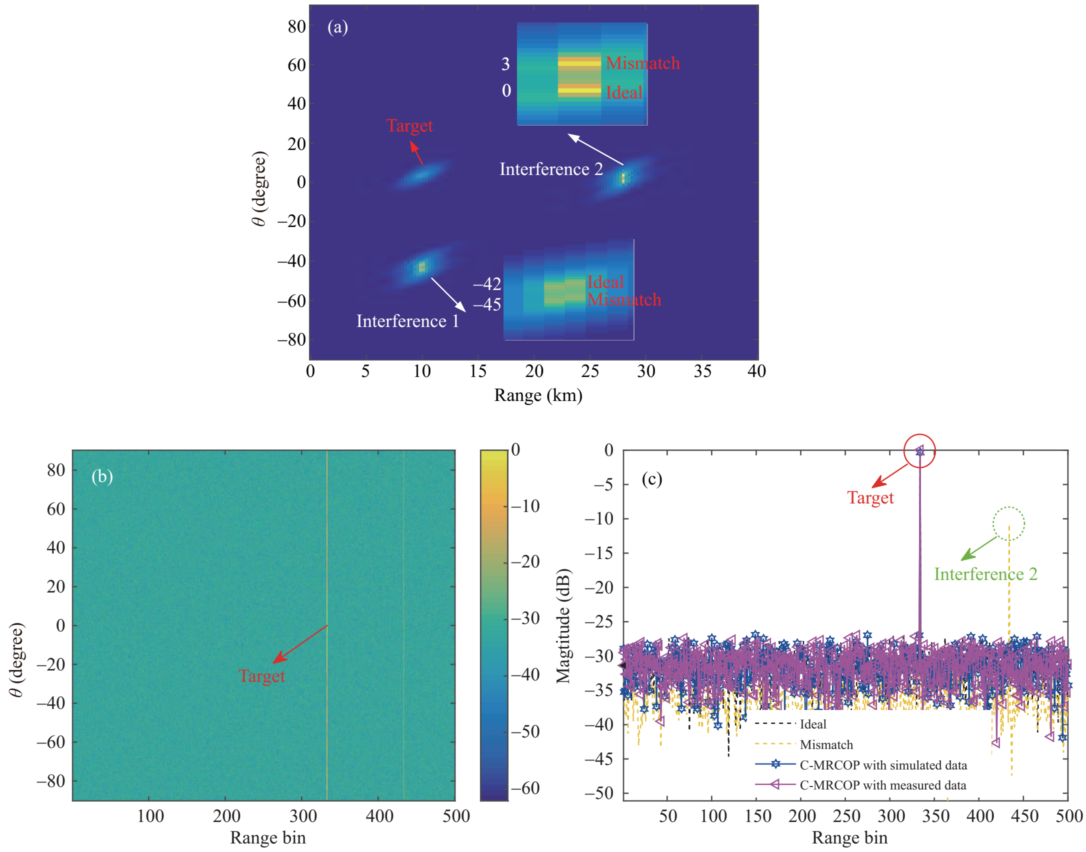

Figure 8 (Color online) Nonstationary interference suppression results with the C-MRCOP method. (a) Capon distribution; (b) matched filtering result in the range-angle domain; (c) matched filtering result at $\theta_0 = 0^\circ$.

interference, the angle $\theta_{j2} = 0^\circ$ and range $R_{j2} = 28$ km are assumed. The moving environment leads to mismatches both in mainlobe and nulling angles. Assume that the mismatched angle is 3°. Shown in Figure 8(a), there are deviations of the positions for the target and interferences in the range-angle domain. Figures 8(b) and (c) illustrate the output of the transmit-receive 2-D matched filtering, where the weight vector is previously devised to obtain the beampattern in Figure 7(a). Assume that the number of range bins is 500, and the range bins of the target and the interferences are 334, 334, and 434. It can be seen in Figure 8(b) that the target is easily detected with the maximum power in the range-angle domain after the transmit-receive 2-D matched filtering, and interferences with angle mismatches are effectively suppressed. The output result in the presence of angle mismatch is presented in Figure 8(c). It is shown that the output power of the interference is high when angle mismatch exists, which in turn generates a high false-alarm ratio. In contrast, by using the C-MRCOP method, the broadened nulls are obtained to suppress the moving interferences adequately, where the output power of interferences can be reduced to a small level. Besides, a flat-top mainlobe is aquired to extend receiving areas for the target, where the response of the target is still constrained to be unity, i,e., $\boldsymbol{w}_{\mathrm{C-MRCOP}}^{\dagger}\boldsymbol{u}_0 = 1$. The measured result shows good agreement with the simulated one, as shown in the Figure 8(c).

6 Conclusion

In this paper, the design of range-angle-dependent transceive beampattern in FDA-MIMO radar has been investigated. At the design stage, methods have been developed to control the responses of the beampattern. In specific, a single response can be adjusted based on weight vector orthogonal decomposition according to a predefined level. Then, for multiple responses, a filtering matrix has been designed by virtue of an oblique projection operator. In this way, iterative algorithms have been proposed by controlling multiple responses either concurrently or successively, termed as C-MRCOP and S-MRCOP, respectively. As a result, the range-angle-dependent transceive beampattern can be formed with a flat-top mainlobe, multiple broadened quasi-nulls, and low sidelobes. At the analysis stage, a comparison of the beampattern performance among different methods including the SDR, the WORD and A^2RC has been done. Moreover, the C-MRCOP method has been applied to the suppression of mainlobe interferences, where angle mismatches both in mainlobe and nulls are involved. Real array antenna measurements have been collected, demonstrating good performance of the designed transceive beampattern and mainlobe interference suppression.

Possible future research studies include designing the weight vector exploiting other methods and accounting for the presence of some specific jammer scenarios.

Acknowledgements This work was supported in part by National Natural Science Foundation of China (Grant Nos. 62101402, 61931016, 62071344), China Postdoctoral Science Foundation (Grant Nos. 2021TQ0261, 2021M702547), Aviation Science Foundation of China (Grant No. 2020000108101), Young Elite Scientists Sponsorship Program by CAST (Grant No. 2021QNRC001), National Key Laboratory of Radar Signal Processing and Science and Technology on Sonar Laboratory (Grant No. 6142109KF212202).

References

1 Nusenu S Y, Wang W Q. Range-dependent spatial modulation using frequency diverse array for OFDM wireless communications. IEEE Trans Veh Technol, 2018, 67: 10886–10895
2 Wang W Q. Overview of frequency diverse array in radar and navigation applications. IET Radar Sonar Nav, 2016, 10: 1001–1012
3 Basit A, Khan W, Khan S, et al. Development of frequency diverse array radar technology: a review. IET Radar Sonar Nav, 2018, 12: 165–175
4 Gui R, Wang W Q, Cui C, et al. Coherent pulsed-FDA radar receiver design with time-variance consideration: SINR and CRB analysis. IEEE Trans Signal Process, 2018, 66: 200–214
5 Basit A, Wang W Q, Nusenu S Y, et al. Range-angle-dependent beampattern synthesis with null depth control for joint radar communication. Antenn Wirel Propag Lett, 2019, 18: 1741–1745
6 Basit A, Wang W Q, Wali S, et al. Transmit beamspace design for FDA-MIMO radar with alternating direction method of multipliers. Signal Process, 2021, 180: 107832
7 Xu Y H, Shi X W, Xu J W, et al. Range-angle-dependent beamforming of pulsed frequency diverse array. IEEE Trans Antenn Propag, 2015, 63: 3262–3267
8 Basit A, Wang W Q, Nusenu S Y. Adaptive transmit beamspace design for cognitive FDA radar tracking. IET Radar Sonar Nav, 2019, 13: 2083–2092
9 Wang W Q, So H C, Farina A. An overview on time/frequency modulated array processing. IEEE J Sel Top Signal Process, 2017, 11: 228–246
10 Fartookzadeh M. Comments on "optimization of sparse frequency diverse array with time-invariant spatial-focusing beampattern". Antenn Wirel Propag Lett, 2018, 17: 2521–2521
11 Yang Y Q, Wang H, Wang H Q, et al. Reply to "comments on 'optimization of sparse frequency diverse array with time-invariant spatial-focusing beampattern'". Antenn Wirel Propag Lett, 2018, 17: 2522–2522
12 Ding Y, Narbudowicz A, Goussetis G. Physical limitation of range-domain secrecy using frequency diverse arrays. IEEE Access, 2020, 8: 63302–63309
13 Nusenu S Y, Huaizong S. Green secure communication range-angle focusing quadrature spatial modulation using frequency modulated diverse retrodirective array for mmWave wireless communications. IEEE Trans Veh Technol, 2019, 68: 6867–6877
14 Xu J W, Liao G S, Zhu S Q, et al. Joint range and angle estimation using MIMO radar with frequency diverse array. IEEE Trans Signal Process, 2015, 63: 3396–3410
15 Huang L B, Zong Z L, Zhang S S, et al. 2-D moving target deception against multichannel SAR-GMTI using frequency diverse array. IEEE Geosci Remote Sens Lett, 2020. doi:10.1109/LGRS.2020.3041296
16 Liu W J, Liu J, Hao C P, et al. Multichannel adaptive signal detection: basic theory and literature review. Sci China Inf Sci, 2022, 65: 121301
17 Xu Y H, Shi X W, Li W T, et al. Low-sidelobe range-angle beamforming with FDA using multiple parameter optimization. IEEE Trans Aerosp Electron Syst, 2019, 55: 2214–2225
18 Lan L, Liao G S, Xu J W, et al. Transceive beamforming with accurate nulling in FDA-MIMO radar for imaging. IEEE Trans Geosci Remote Sens, 2020, 58: 4145–4159
19 Yu X X, Cui G L, Yang J, et al. Wideband MIMO radar beampattern shaping with space-frequency nulling. Signal Process, 2019, 160: 80–87
20 Liao B, Cui G L, Huang L, et al. Robust adaptive beamforming with precise main beam control. IEEE Trans Aerosp Electron Syst, 2017, 53: 345–356
21 Liao B, Cui G L, Huang L, et al. Robust adaptive beamforming with random steering vector mismatch. Signal Process, 2016, 129: 190–194
22 Yu X X, Cui G L, Yang J, et al. MIMO radar transmit-receive design for moving target detection in signal-dependent clutter. IEEE Trans Veh Technol, 2020, 69: 522–536
23 Fuchs B. Application of convex relaxation to array synthesis problems. IEEE Trans Antenn Propag, 2014, 62: 634–640
24 Liao B, Tsui K M, Chan S C. Robust beamforming with magnitude response constraints using iterative second-order cone programming. IEEE Trans Antenn Propag, 2011, 59: 3477–3482
25 Luo Z Q, Ma W K, So A M C, et al. Semidefinite relaxation of quadratic optimization problems. IEEE Signal Process Mag, 2010, 27: 20–34
26 Yang X P, Zhang Z A, Zeng T, et al. Mainlobe interference suppression based on eigen-projection processing and covariance matrix reconstruction. Antenn Wirel Propag Lett, 2014, 13: 1369–1372
27 Feng Y, Liao G S, Xu J W, et al. Robust adaptive beamforming against large steering vector mismatch using multiple uncertainty sets. Signal Process, 2018, 152: 320–330
28 Sureau J C, Keeping K. Sidelobe control in cylindrical arrays. IEEE Trans Antenn Propag, 1982, 30: 1027–1031
29 Olen C A, Compton R T. A numerical pattern synthesis algorithm for arrays. IEEE Trans Antenn Propag, 1990, 38: 1666–1676
30 Zhang X J, He Z S, Xia X G, et al. OPARC: optimal and precise array response control algorithm — part I: fundamentals. IEEE Trans Signal Process, 2019, 67: 652–667

31 Zhang X J, He Z S, Xia X G, et al. OPARC: optimal and precise array response control algorithm — part II: multi-points and applications. IEEE Trans Signal Process, 2019, 67: 668–683
32 Zhang X J, He Z S, Liao B, et al. A^2RC: an accurate array response control algorithm for pattern synthesis. IEEE Trans Signal Process, 2017, 65: 1810–1824
33 Zhang X J, He Z S, Liao B, et al. Pattern synthesis for arbitrary arrays via weight vector orthogonal decomposition. IEEE Trans Signal Process, 2018, 66: 1286–1299
34 Chen K S, Yun X H, He Z J, et al. Synthesis of sparse planar arrays using modified real genetic algorithm. IEEE Trans Antenn Propag, 2007, 55: 1067–1073
35 Boeringer D W, Werner D H. Particle swarm optimization versus genetic algorithms for phased array synthesis. IEEE Trans Antenn Propag, 2004, 52: 771–779
36 Murino V, Trucco A, Regazzoni C S. Synthesis of unequally spaced arrays by simulated annealing. IEEE Trans Signal Process, 1996, 44: 119–122
37 Lan L, Xu J W, Liao G S, et al. Suppression of mainbeam deceptive jammer with FDA-MIMO radar. IEEE Trans Veh Technol, 2020, 69: 11584–11598
38 Behrens R T, Scharf L L. Signal processing applications of oblique projection operators. IEEE Trans Signal Process, 1994, 42: 1413–1424
39 Amar A, Doron M A. A linearly constrained minimum variance beamformer with a pre-specified suppression level over a pre-defined broad null sector. Signal Process, 2015, 109: 165–171
40 Frost O L. An algorithm for linearly constrained adaptive array processing. Proc IEEE, 1972, 60: 926–935

Appendix A Derivations of the received signals after matched filtering

The received signals in (2) are firstly multiplied by $\mathrm{e}^{-\mathrm{j}2\pi f_0 t}$. Then, on each receive channel, the echo is digitally mixed with $\mathrm{e}^{-\mathrm{j}2\pi(l-1)\Delta f t}$, it yields,

$$\bar{y}_n(t,\theta_0)=\alpha_0\mathrm{e}^{\mathrm{j}2\pi\frac{d}{\lambda}(n-1)\sin(\theta_0)}\mathrm{e}^{-\mathrm{j}2\pi\Delta f(l-1)t}\sum_{m=1}^{M}\phi_m(t-\tau_0)\mathrm{e}^{\mathrm{j}2\pi\Delta f(m-1)(t-\tau_0)}\mathrm{e}^{\mathrm{j}2\pi\frac{d}{\lambda}(m-1)\sin(\theta_0)}. \tag{A1}$$

Then, it passes through a bank of matched filters, where the output of the n-th received signal from the l-th filter, i.e., $h_l(t)=\phi_l^*(-t)$, is expressed as

$$\begin{aligned}\hat{y}_n(t,\theta_0)&=\int_{-\infty}^{\infty}\bar{y}_n(t,\theta_0)h_l\left(t-\tau\right)\mathrm{d}\tau\\&=\alpha_0\mathrm{e}^{\mathrm{j}2\pi\frac{d}{\lambda}(n-1)\sin(\theta_0)}\sum_{m=1}^{M}\mathrm{e}^{\mathrm{j}2\pi\frac{d}{\lambda}(m-1)\sin(\theta_0)}\int_{-\infty}^{\infty}\phi_m(\tau-\tau_0)\phi_l^*\left(\tau-t\right)\mathrm{e}^{\mathrm{j}2\pi\Delta f(m-1)(\tau-\tau_0)}\mathrm{e}^{-\mathrm{j}2\pi\Delta f(l-1)\tau}\mathrm{d}\tau\\&\overset{s=\tau-\tau_0}{=}\alpha_0\mathrm{e}^{\mathrm{j}2\pi\frac{d}{\lambda}(n-1)\sin(\theta_0)}\mathrm{e}^{-\mathrm{j}2\pi\Delta f(l-1)\tau_0}\sum_{m=1}^{M}\mathrm{e}^{\mathrm{j}2\pi\frac{d}{\lambda}(m-1)\sin(\theta_0)}\chi_{l,m}\left(t-\tau_0,(m-l)\Delta f\right),\end{aligned}\tag{A2}$$

where the cross-ambiguity function is defined as

$$\begin{aligned}\chi_{l,m}\left(t-\tau_0,(m-l)\Delta f\right)&=\int_{-\infty}^{\infty}\phi_m(s)\phi_l^*\left(s-(t-\tau_0)\right)\mathrm{e}^{\mathrm{j}2\pi\Delta f(m-l)s}\mathrm{d}s\\&\approx\int_0^{T_p}\phi_m\left(s\right)\phi_l^*\left(s\right)\mathrm{d}s=R_{l,m},\end{aligned}\tag{A3}$$

where the approximations rely on the use of pulses whose cross-ambiguities is Doppler tolerant, i.e., the ambiguity function exhibits a flat behavior in a neighbourhood of the origin (0,0). Assume that the transmitted waveforms are orthogonal, i.e., $R_{l,m}=\begin{cases}1, m=l,\\0, m\neq l,\end{cases}$ the n-th signal after matched filtered with the l-th waveform is expressed as

$$\hat{y}_n(t,\theta_0)=\alpha_0\mathrm{e}^{\mathrm{j}2\pi\frac{d}{\lambda}(n-1)\sin(\theta_0)}\mathrm{e}^{-\mathrm{j}2\pi\Delta f(l-1)\tau_0}\mathrm{e}^{\mathrm{j}2\pi\frac{d}{\lambda}(l-1)\sin(\theta_0)}. \tag{A4}$$

It can be seen that $\hat{y}_n(t,\theta_0)$ is time-independent. Subsequently, the received signals from the n-th element can be expressed in an $M\times 1$-vector form as

$$\boldsymbol{y}_{n,m}=\left[\hat{y}_{n,1}\left(t,\theta_0\right),\hat{y}_{n,2}\left(t,\theta_0\right),\ldots,\hat{y}_{n,M}\left(t,\theta_0\right)\right]^{\mathrm{T}}=\alpha_0\boldsymbol{a}_{\mathrm{T}}\left(R_0,\theta_0\right)\mathrm{e}^{\mathrm{j}2\pi\frac{d}{\lambda}(n-1)\sin(\theta_0)}. \tag{A5}$$

Hence, the overall received signal is obtained by stacking the output of the correlators into an $M^2\times 1$-dimensional vector as

$$\begin{aligned}\boldsymbol{y}_{\mathrm{s}}&=\left[\boldsymbol{y}_1\left(t,\theta_0\right),\boldsymbol{y}_2\left(t,\theta_0\right),\ldots,\boldsymbol{y}_M\left(t,\theta_0\right)\right]^{\mathrm{T}}\\&=\alpha_0\boldsymbol{b}_{\mathrm{R}}\left(\theta_0\right)\otimes\boldsymbol{a}_{\mathrm{T}}\left(R_0,\theta_0\right).\end{aligned}\tag{A6}$$

Appendix B Proof for proposition 1

Substituting $\alpha_l=\frac{1}{\boldsymbol{u}_0^{\dagger}\boldsymbol{w}_{\perp}+\beta_l\boldsymbol{u}_0^{\dagger}\boldsymbol{w}_{\parallel}}$ into (15), we have the equation as

$$\begin{aligned}&\frac{\beta_l^2\boldsymbol{w}_{\parallel}^{\dagger}\boldsymbol{u}_l\boldsymbol{u}_l^{\dagger}\boldsymbol{w}_{\parallel}}{(\boldsymbol{u}_0^{\dagger}\boldsymbol{w}_{\perp}+\beta_l\boldsymbol{u}_0^{\dagger}\boldsymbol{w}_{\parallel})^{\dagger}(\boldsymbol{u}_0^{\mathrm{H}}\boldsymbol{w}_{\perp}+\beta_l\boldsymbol{u}_0^{\dagger}\boldsymbol{w}_{\parallel})}=\xi,\\&\beta_l^2\boldsymbol{w}_{\parallel}^{\dagger}\boldsymbol{u}_l\boldsymbol{u}_l^{\dagger}\boldsymbol{w}_{\parallel}=\xi(\boldsymbol{u}_0^{\dagger}\boldsymbol{w}_{\perp}+\beta_l\boldsymbol{u}_0^{\mathrm{H}}\boldsymbol{w}_{\parallel})^{\dagger}(\boldsymbol{u}_0^{\dagger}\boldsymbol{w}_{\perp}+\beta_l\boldsymbol{u}_0^{\dagger}\boldsymbol{w}_{\parallel}),\\&\beta_l^2(\boldsymbol{w}_{\parallel}^{\dagger}\boldsymbol{u}_l\boldsymbol{u}_l^{\dagger}\boldsymbol{w}_{\parallel}-\xi\boldsymbol{w}_{\parallel}^{\dagger}\boldsymbol{u}_0\boldsymbol{u}_0^{\dagger}\boldsymbol{w}_{\parallel})-\beta_l\xi(\boldsymbol{w}_{\perp}^{\dagger}\boldsymbol{u}_0\boldsymbol{u}_0^{\dagger}\boldsymbol{w}_{\parallel}+\boldsymbol{w}_{\parallel}^{\dagger}\boldsymbol{u}_0\boldsymbol{u}_0^{\dagger}\boldsymbol{w}_{\perp})-\xi\boldsymbol{w}_{\perp}^{\dagger}\boldsymbol{u}_0\boldsymbol{u}_0^{\dagger}\boldsymbol{w}_{\perp}=0.\end{aligned}\tag{B1}$$

We find that Eq. (44) is a quadratic equation about β_l. For simplicity, define $a_1 \triangleq \boldsymbol{w}_\parallel^\dagger \boldsymbol{u}_l \boldsymbol{u}_l^\dagger \boldsymbol{w}_\parallel$, $a_2 \triangleq \xi \boldsymbol{w}_\parallel^\dagger \boldsymbol{u}_0 \boldsymbol{u}_0^\dagger \boldsymbol{w}_\parallel$, $a_3 \triangleq \xi \boldsymbol{w}_\perp^\dagger \boldsymbol{u}_0 \boldsymbol{u}_0^\dagger \boldsymbol{w}_\parallel$, $a_4 \triangleq \xi \boldsymbol{w}_\parallel^\dagger \boldsymbol{u}_0 \boldsymbol{u}_0^\dagger \boldsymbol{w}_\perp$, and $a_5 \triangleq \xi \boldsymbol{w}_\perp^\dagger \boldsymbol{u}_0 \boldsymbol{u}_0^\dagger \boldsymbol{w}_\perp$. Eq. (44) is further abstracted into a mathematical problem as

$$\beta_l^2 \left(a_1 - a_2\right) - \beta_l \left(a_3 + a_4\right) - a_5 = 0. \tag{B2}$$

Calculating the discriminant in (45), it is expressed as

$$\begin{aligned}\Delta &= \left(a_3 + a_4\right)^2 + 4a_5 \left(a_1 - a_2\right) \\ &= 4\xi \boldsymbol{w}_\parallel^\dagger \boldsymbol{u}_l \boldsymbol{u}_l^\dagger \boldsymbol{w}_\parallel \boldsymbol{w}_\perp^\dagger \boldsymbol{u}_0 \boldsymbol{u}_0^\dagger \boldsymbol{w}_\perp \\ &= 4\xi |\boldsymbol{w}_\parallel^\dagger \boldsymbol{u}_l|^2 |\boldsymbol{w}_\perp^\dagger \boldsymbol{u}_0|^2 \geqslant 0. \end{aligned} \tag{B3}$$

Hence, the solutions to (47) are derived as

$$\breve{\beta}_l^1 = \frac{\left(a_3 + a_4\right) + \sqrt{\Delta}}{2\left(a_1 - a_2\right)}, \tag{B4a}$$

$$\breve{\beta}_l^2 = \frac{\left(a_3 + a_4\right) - \sqrt{\Delta}}{2\left(a_1 - a_2\right)}. \tag{B4b}$$